JOURNAL OF COMPUTATIONAL PHYSICS **145,** 246–279 (1998)
ARTICLE NO. CP986006

Numerical Simulation of Randomly Forced Turbulent Flows

L. Machiels* and M. O. Deville

Fluid Mechanics Laboratory, Swiss Federal Institute of Technology, CH-1015, Lausanne, Switzerland

Received August 26, 1997

Several authors have proposed studying randomly forced turbulent flows (e.g., E. A. Novikov, *Soviet Physics JETP*, **20**(5), 1290 1965). More recently, theoretical investigations (e.g., renormalization group) have focused on white-noise forced Navier–Stokes equations (V. Yakhot and S. A. Orszag, *J. Sci. Comput.* **1**(1), 3 1986). The present article aims to provide an appropriate numerical method for the simulation of randomly forced turbulent systems. The spatial discretization is based on the classical Fourier spectral method. The time integration is performed by a second-order Runge–Kutta scheme. The consistency of an extension of this scheme to treat additive noise stochastic differential equations is proved. The random number generator is based on lagged Fibonacci series. Results are presented for two randomly forced problems: the Burgers and the incompressible Navier–Stokes equations with a white-noise in time forcing term characterized by a power-law correlation function in spectral space. A variety of statistics are computed for both problems, including the structure functions. The third-order structure functions are compared with their exact expressions in the inertial subrange. The influence of the dissipation mechanism (viscous or hyperviscous) on the inertial subrange is discussed. In particular, probability density functions of velocity increments are computed for the Navier–Stokes simulation. Finally, for both Burgers and Navier–Stokes problems, our results support the view that random sweeping is the dominant effect of the large-scale motion on the small-scales.

1. INTRODUCTION

Turbulence is a non-equilibrium phenomenon: if a turbulent flow is left in a domain without any external injection of energy, it decays. To prevent this decay and achieve a statistically steady state in which mean quantities are independent of time, one can impose boundary conditions on the velocity field. In that case, the flow is inhomogeneous and

*Present address: Massachusetts Institute of Technology, Room 3-243, 77 Massachusetts Avenue, Cambridge, MA 02139. E-mail: machiels@mit.edu.

0021-9991/98 $25.00

complex. Understanding the properties of such flows remains a major challenge. Another way to achieve a statistically steady state while preserving homogeneity and eventually isotropy of turbulence is to add (following Novikov's suggestion [1]) a random forcing term in the equations. This forced-dissipative system will give a description of the essential nonlinear processes in a turbulent fluid divorced from any peculiarities induced by the boundary or initial conditions.

During the past decades, forced homogeneous turbulence has received much attention. In the theory of turbulence, methods based on renormalization of diagrammatic expansions have been investigated thoroughly [2]. The renormalization group (RG) approaches (see, e.g., [3–8]) belong to the same family of theories. In the field of computer simulations, since the pioneering work of Orszag and Patterson [9], many simulations of homogeneous turbulence have been performed. Some of these studies have treated the decay of turbulence from given initial conditions. Others showed results for forced turbulence (see, e.g., [10–12]). The forcing is active only in a narrow band of wave-numbers located near the origin. Different types of forcing terms (deterministic or stochastic) were used. Most of the authors came to the conclusion that the dynamics of the inertial subrange scales (defined as the subrange of scales of motion for which the fluid is effectively described by the inviscid equations), seems to be independent of the exact form of the forcing. Siggia [10] mentioned that this may be demonstrated, in principle, using a renormalization group analysis.

More recently, simulations of homogeneous turbulence have been performed replacing the classical Laplacian dissipation by a higher order term [13, 14]. Using this technique, one hopes to broaden the inertial subrange and obtain solutions closer to high Reynolds number turbulence while keeping the number of degrees of freedom to a reasonable value. There is also a theoretical issue related to hyperviscous turbulent flows. Leveque and She [15] have shown the nonuniversality of the inertial subrange of a Gledzer–Ohkitani–Yamada (GOY) shell model with respect to the hyperviscosity exponent. This phenomenon may be related, in RG terminology, to an infinite set of fixed points (Eyink [16]).

The RG method applied to turbulence by Yakhot and Orszag [7] has stimulated the study of a new type of forced homogeneous turbulence. Their theory predicts critical exponents and quantities such as the Kolmogorov constant and the velocity derivative skewness (Smith and Reynolds [17]) for a statistically isotropic flow sustained by white-noise Gaussian stochastic forcing defined by a power-law covariance operator in Fourier space. According to the theory, the Kolmogorov–Obukhov $-5/3$ law for the energy spectrum is recovered when the forcing correlation functions scale like k^{-3} in three dimensions (k is the wave-number). The Yakhot and Orszag theory is based on the postulate that this particular forced-dissipative model is a good candidate for representing the small-scales of real turbulence. The value of the Kolmogorov constant, $C_K = 1.6$, predicted by the theory is close to experimental results which is remarkable in view of the various assumptions used in its derivation. An interesting feature of the theory is the prediction of an Eulerian energy frequency spectrum which scales like ω^{-2} (ω is the time frequency) [18]. This is in contradiction with the classical view of considering the random sweeping as the dominant interaction between large-scales and small-scales [19–21]. The work of Yakhot and Orszag leads to an investigation of other forced-dissipative systems like the random-force-driven Burgers equation [22, 23]. For this system, a random force with a k^{-1} power-law covariance operator results in a Kolmogorov energy spectrum.

The analysis of Yakhot and Orszag raises new important questions on the route towards a better understanding of homogeneous turbulence. Some of these questions can be answered

by numerical experiments. Among them, one might ask: What are the statistical properties of a turbulence with a k^{-3} force term? Are they close to the properties of large-scale forced turbulence? (This question has been partially answered by Migdal *et al.* [24] who were able to show, using an infrared renormalization, that the k^{-3} forcing comes as an intrinsic reaction of turbulence to the large-scale forcing.) Are the quantities predicted by the theory in good agreement with numerical results? Can we give quantitative evaluations of the assumptions used in the derivation of the theory (among theses assumptions, one finds the truncation to second-order corrections of the parameters and the distant interaction limit)? To answer some of these questions, numerical simulations of randomly forced turbulence have already been performed [25]. However, a thorough analysis is lacking. (Note that, randomly forced turbulence appears also in the context of large eddy simulations when the backscatter effect is represented by a stochastic term [26, 27].)

Therefore, there is a strong motivation for a numerical study of a family of randomly forced turbulent flows characterized by power-law force correlations. The main point of this article is to present a numerical method to solve efficiently problems of this family. In particular, we make use of a Runge–Kutta time marching scheme for additive noise stochastic differential equations which is second-order accurate in the weak sense (see the definition of weak convergence in Section 3). The spatial discretization is based on the classical Fourier spectral algorithm. Due to the Runge–Kutta method, two evaluations of these terms are necessary per time step. Therefore the dealiasing can be achieved without any extra cost by a random-shifting technique [28]. Another important issue is the generation of pseudorandom numbers to build up the stochastic forcing. Two important properties are required. Firstly, the period of the generator should be large enough to ensure statistically independent forcing increments. Secondly, we desire a generator which is computationally efficient on a vector computer. We recommend a generator based on lagged Fibonacci series which combines both properties [29–31].

Two problems have retained our attention: the one-dimensional Burgers equation and the three-dimensional incompressible Navier–Stokes equations. Each of them is defined on a periodic domain (an interval for Burgers and a cube for Navier–Stokes). The viscous Burgers problem is solved with a resolution of 32,768 modes for a white-noise in time force with a k^{-1} power-law correlation function [22, 23]. The viscous and hyperviscous Navier–Stokes problems are solved with a resolution of 256^3 modes for a k^{-3} forcing term [7, 25].

The paper is organized as follows. In Section 2, random force turbulent models are presented for the Burgers and Navier–Stokes equations. The consistency of the second-order stochastic Runge–Kutta scheme is proved in Section 3. Section 4 deals with the description of the discretization technique, the random number generator algorithm, and the computational performances of the Navier–Stokes solver. Various results for the stochastic Burgers and Navier–Stokes equations are discussed in Section 5. Finally, Section 6 draws some conclusions.

2. PRESENTATION OF THE PROBLEMS

We consider two problems, namely the Burgers and Navier–Stokes equations with stochastic, white-noise in time, forcing terms. The velocity field, solution of one of these problems, can be written in the form of an Ito stochastic process $v(t) = \{v(x, t), x \in \mathcal{D}\}$. Here, $t \geq 0$

and $\mathcal{D}$ is the spatial domain. For instance for the one-dimensional Burgers equation, we have

$$v(x,t) = v(x,0) + \int_0^t \left[-v(x,s)\frac{\partial v}{\partial x}(x,s) + \nu \frac{\partial^2 v}{\partial x^2}(x,s) \right] ds + \int_0^t dw(x,s), \quad (1)$$

where ν is the kinematic viscosity. The second integral is usually refereed to as the Ito stochastic integral with respect to the Wiener process $w(t) = \{w(x,t), x \in \mathcal{D}\}$. Recall that a Wiener process is a stochastic process defined by the three following properties

(i) $w(0) = 0$;

(ii) $w(t)$ is a continuous function of t;

(iii) the increments $\{w(t+\Delta t) - w(t), t \geq 0, \Delta t > 0\}$ are independent of each other and have a Gaussian probability distribution with a zero mean and a variance of the form $\langle (w(x', t+\Delta t) - w(x,t))^2 \rangle = \Delta t F(x,x')$ where the symbol $\langle \cdot \rangle$ denotes the ensemble average and $F(x,x')$ is the covariance function.

The integral equation (1) may be written in its differential form

$$dv(x,t) = -v(x,t)\frac{\partial v}{\partial x}(x,t)\,dt + \nu \frac{\partial^2 v}{\partial x^2}(x,t)\,dt + dw(x,t),$$

or in the more common form

$$\frac{\partial v}{\partial t}(x,t) + v(x,t)\frac{\partial v}{\partial x}(x,t) = \nu \frac{\partial^2 v}{\partial x^2}(x,t) + f(x,t), \quad (2)$$

where $f(x,t)$ is the so-called white-noise force term and is the generalized derivative of the Wiener process $w(x,t)$.

Due to point (iii) in the above definition, the white-noise is not continuous in time and the classical Taylor expansion analysis used to prove the consistency of numerical approximation schemes does not apply to this kind of equation. Nevertheless, various schemes have been designed for stochastic differential equation based on an Ito–Taylor expansion [32]. Section 3 is devoted to this subject.

We will also consider replacing the normal Laplacian dissipation

$$\nu \frac{\partial^2 v}{\partial x^2}(x,t),$$

by a higher power of the Laplacian

$$(-1)^{h+1}\nu_h \frac{\partial^{2h} v}{\partial x^{2h}}(x,t),$$

where h is an integer. The hyperviscous dissipation concentrates the energy sink at the small-scales leading to an enhanced inertial subrange. In addition to this practical motivation for studying hyperviscous systems, there is also a theoretical interest as mentioned in the Introduction.

The aim of the two sections below is to state precisely the different problems treated in this article. Essentially, we specify the two-point correlation functions of the forcing terms in spectral space and in physical space for an infinite domain. Afterwards, we show that the length scale associated with the external forcing allows us to define an approximate discrete finite-size problem.

2.1. *Burgers*

In physical space, the Burgers equation is given by Eq. (2). We will consider the homogeneous case where the domain $\mathcal{D} =]-\infty, +\infty[$ and $0 \le t < +\infty$ (the intial condition being $v(x, 0) = 0$). According to the following Fourier transform

$$\hat{v}(k, t) = \int_{-\infty}^{+\infty} v(x, t)\, e^{-ikx}\, dx,$$
$$v(x, t) = \frac{1}{2\pi} \int_{-\infty}^{+\infty} \hat{v}(k, t)\, e^{ikx}\, dk,$$

the equation reads, in spectral space,

$$\left(\partial_t + \nu k^2\right)\hat{v}(k, t) = \hat{f}(k, t) - \frac{ik}{2(2\pi)} \int_{-\infty}^{+\infty} \hat{v}(p, t)\hat{v}(k - p, t)\, dp. \tag{3}$$

This equation will be restricted to the wave-number domain $\mathcal{D}_r = \{k \in \mathcal{D} \mid k_o \le |k| \le k_d\}$ where k_o and k_d designate the infrared and the ultraviolet cutoffs, respectively. The ultraviolet cutoff is taken in the range of wave-numbers where the dynamics is dominated by the viscous dissipation.

In the subsequent paragraphs, we define different quantities such as the mean energy and the mean dissipation rate. Afterwards, we specify the external forcing and its relation with the mean dissipation rate. We will show that its correlation length scale is smaller than the domain size of the discrete problem. Finally, in the last paragraph, we discuss briefly the meaning of the limit case $k_o \to 0$.

For problem (2), the mean energy $E(t)$ and the mean dissipation rate $\varepsilon(t)$ defined respectively by

$$E(t) = \frac{1}{2}\langle v(x, t)^2 \rangle, \qquad \text{and} \qquad \varepsilon(t) = \nu \left\langle \left(\frac{\partial v(x, t)}{\partial x} \right)^2 \right\rangle,$$

are related by the equation

$$\frac{dE(t)}{dt} = \frac{1}{4(2\pi)^2} \int_{\mathcal{D}_r} dk \int_{\mathcal{D}_r} dk' [\langle \hat{f}(k, t)\hat{v}(k', t) \rangle + \langle \hat{f}(k', t)\hat{v}(k, t) \rangle] - \varepsilon(t).$$

This equation is deduced from (3). Since the velocity field is assumed to be statistically homogeneous, the mean quantities do not depend on the space variable. Assuming that, after a time $t^* > 0$, the system reaches a statistical steady state, we have, for all $t > t^*$, $dE(t)/dt = 0$ and

$$\varepsilon = \frac{1}{4(2\pi)^2} \int_{\mathcal{D}_r} dk \int_{\mathcal{D}_r} dk' [\langle \hat{f}(k, t)\hat{v}(k', t) \rangle + \langle \hat{f}(k', t)\hat{v}(k, t) \rangle]. \tag{4}$$

The forcing term is defined by the following correlation function

$$\langle \hat{f}(k', t')\, \hat{f}(k, t) \rangle = (2\pi)\hat{F}(k)\delta(k + k')\delta(t - t') \qquad \text{for } k \in \mathcal{D}_r, \tag{5}$$

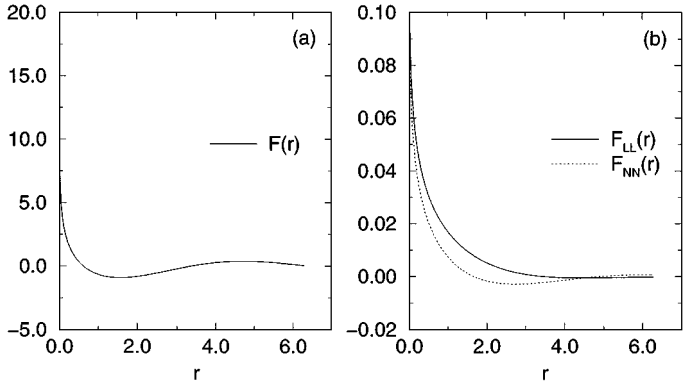

FIG. 1. Two-point correlation functions of the stochastic forcing: (a) Burgers; (b) Navier–Stokes.

where $\hat{F}(k) = 2D|k|^{-1}$ and $D = D(\varepsilon, k_o, k_d)$ is a function of ε, k_o, and k_d. Using Novikov's theorem [1]

$$\langle \hat{f}(k,t)\hat{v}(k,t)\rangle = \frac{2\pi}{2}\delta(k+k')\hat{F}(k),$$

and by virtue of Eq. (4), we find

$$D(\varepsilon, k_o, k_d) = \frac{2\pi\varepsilon}{\ln(k_d/k_o)} \qquad \text{and} \qquad \hat{F}(k) = \frac{2\pi\varepsilon|k|^{-1}}{\ln(k_d/k_o)}. \tag{6}$$

In physical space, the two-point correlation function of the forcing is defined by

$$\langle f(x+r, t+\tau)\, f(x,t)\rangle = F(r)\delta(\tau),$$

where the function $F(r)$ is the inverse Fourier transform of $\hat{F}(k)$ given by

$$F(r) = \frac{2\varepsilon(\mathrm{ci}(k_d r) - \mathrm{ci}(k_o r))}{\ln(k_d/k_o)}, \tag{7}$$

where ci$(\cdot)$ denotes the cosine integral. Figure 1(a) shows the function $F(r)$ for $k_o = 1$, $k_d = 16{,}384$, and $\varepsilon = 10$ which are approximately the values used in the simulation (see Subsection 5.1). The function $F(r)$ is very sharp near $r = 0$ ($F(0) = 20$). The maximum amplitude between π and 2π is very small compared to $F(0)$; this means that the correlation of the forcing for $r > \pi$ is weak and a simulation performed in a finite periodic domain of size 2π will be a good approximation of the original problem defined on an infinite size domain.

It is interesting to consider the limit $k_o \to 0$ while ε is kept constant. In that limit $F(r) = F(0) = 2\epsilon$ and the differential length scale associated to the forcing

$$\lambda_f = \left(-\frac{F(0)}{2F''(0)}\right)^{1/2} = \left(\frac{\ln(k_d/k_o)}{k_d^2 - k_o^2}\right)^{1/2},$$

is infinite. This is the Burgers equivalent for Novikov's turbulence [1] (see the definition of Novikov's turbulence in Subsection 2.2). In spectral space, one can easily show that

$$\hat{F}(k) = 2\varepsilon\delta(k). \tag{8}$$

Therefore the forcing is singular in this limit. The k^{-1} forcing can be interpreted as a regularization of an infrared divergent forcing. In that context, k_o is the regularization parameter. The regularized forcing has a finite characteristic length scale which allows us to restrict ourselves to a finite size domain as shown in the previous paragraph. We notice that since the mode $k = 0$ does not exchange energy with other modes, the Burgers equation, along with the forcing (8), will accumulate energy in the zero wave-number and the cascade of energy across wave-numbers will not take place. The case $k_o \to 0^+$ where $k_o > 0$ is more interesting. The behavior of this system depends on the regularization procedure and is fundamentally different from the pure $\delta(k)$ forcing case since it corresponds to a constant flux of energy across the wave-numbers. The limit case $k_o \to 0^+$ is an anomaly in the terminology of field theory. It has been shown by Chekhlov [33] both theoretically, using second-order RG approximations, and experimentally, in a simulation with hyperviscous dissipation, that the regularized k^{-1} forced problem shows also a scale-invariant Kolmogorov $-5/3$ spectrum. (Note that, for the Burgers problem defined on a finite size domain, it is known that a constant energy flux solution, obtained by injecting energy at low wave-numbers, leads to a k^{-2} spectrum.)

2.2. *Navier–Stokes*

The Navier–Stokes problem is the generalization of the Burgers problem in three dimensions with, in addition, a pressure term and the incompressibility constraint,

$$\frac{\partial v_\alpha}{\partial t}(\boldsymbol{x}, t) + v_\beta(\boldsymbol{x}, t)\frac{\partial v_\alpha}{\partial x_\beta}(\boldsymbol{x}, t) = f_\alpha(\boldsymbol{x}, t) - \frac{\partial p}{\partial x_\alpha}(\boldsymbol{x}, t) + \nu\frac{\partial^2 v_\alpha}{\partial x_\beta \partial x_\beta}(\boldsymbol{x}, t),$$

$$\frac{\partial v_\alpha}{\partial x_\alpha}(\boldsymbol{x}, t) = 0.$$

In this equation, $v_\alpha(\boldsymbol{x}, t)$ ($\alpha = 1, 2, 3$) and $p(\boldsymbol{x}, t)$ are respectively the velocity and pressure fields, $f_\alpha(\boldsymbol{x}, t)$ is the white-noise forcing, and the summation convention of repeated indices has been applied. The problem is defined on the domain $\mathcal{D} =]-\infty, +\infty[^3$ and for $0 < t < \infty$ with the initial condition $v_\alpha(\boldsymbol{x}, 0) = 0$. Given the following Fourier transform

$$\hat{v}_\alpha(\boldsymbol{k}, t) = \int_{\mathcal{D}} v_\alpha(\boldsymbol{x}, t)\, e^{-i\boldsymbol{k}\cdot\boldsymbol{x}}\, d^3x,$$

$$v_\alpha(\boldsymbol{x}, t) = \frac{1}{(2\pi)^3}\int_{\mathcal{D}} \hat{v}_\alpha(\boldsymbol{k}, t)\, e^{i\boldsymbol{k}\cdot\boldsymbol{x}}\, d^3k,$$

one may write the Navier–Stokes equations in spectral formulation

$$\left(\partial_t + \nu k^2\right)\hat{v}_\alpha(\boldsymbol{k}, t) = \hat{f}_\alpha(\boldsymbol{k}, t) - \frac{i}{2(2\pi)^3}P_{\alpha\beta\gamma}(\boldsymbol{k})\int_{\mathcal{D}} \hat{v}_\beta(\boldsymbol{p}, t)\hat{v}_\gamma(\boldsymbol{k} - \boldsymbol{p}, t)\, d^3p,$$

where

$$P_{\alpha\beta\gamma}(\boldsymbol{k}) = k_\beta P_{\alpha\gamma}(\boldsymbol{k}) - k_\gamma P_{\alpha\beta}(\boldsymbol{k}),$$

and

$$P_{\alpha\beta}(\boldsymbol{k}) = \delta_{\alpha\beta} - k_\alpha k_\beta/(k_\gamma k_\gamma). \tag{9}$$

The projector $P_{\alpha\beta}(\boldsymbol{k})$ eliminates the pressure. As for the Burgers problem, we restrict the wave-number domain to $\mathcal{D}_r = \{\boldsymbol{k} \in \mathcal{D} \mid k = (k_\alpha k_\alpha)^{1/2} \in [k_o, k_d]\}$.

The force term is defined by the following correlation functions

$$\langle \hat{f}_\alpha(\boldsymbol{k}', t')\, \hat{f}_\beta(\boldsymbol{k}, t)\rangle = (2\pi)^3 P_{\alpha\beta}(\boldsymbol{k})\hat{F}(k)\delta(\boldsymbol{k}+\boldsymbol{k}')\delta(t-t'),$$

where $\hat{F}(k) = 2D|k|^{-3}$. If we assume that after a time t^*, the system reaches a statistically steady state, D can be related to ε, k_o, and k_d using Novikov's theorem [1]. For the Navier–Stokes problem, the mean dissipation rate is defined by

$$\varepsilon = \nu\left[2\left\langle\left(\frac{\partial v_1}{\partial x_1}\right)^2\right\rangle + 2\left\langle\left(\frac{\partial v_2}{\partial x_2}\right)^2\right\rangle + 2\left\langle\left(\frac{\partial v_3}{\partial x_3}\right)^2\right\rangle + \left\langle\left(\frac{\partial v_2}{\partial x_1}+\frac{\partial v_1}{\partial x_2}\right)^2\right\rangle + \left\langle\left(\frac{\partial v_3}{\partial x_2}+\frac{\partial v_2}{\partial x_3}\right)^2\right\rangle + \left\langle\left(\frac{\partial v_1}{\partial x_3}+\frac{\partial v_3}{\partial x_1}\right)^2\right\rangle\right].$$

We find the following expressions for D and $\hat{F}$

$$D(\varepsilon, k_o, k_d) = \frac{\pi^2\epsilon}{\ln(k_d/k_o)}, \qquad \text{and} \qquad \hat{F}(k) = \frac{2\pi^2\varepsilon|k|^{-3}}{\ln(k_d/k_o)}. \tag{10}$$

In physical space, the two-point correlation functions of the forcing term are given by

$$\langle f_\alpha(\boldsymbol{x}+\boldsymbol{r}, t+\tau)\, f_\beta(\boldsymbol{x}, t)\rangle = F_{\alpha\beta}(\boldsymbol{r})\delta(\tau), \tag{11}$$

where

$$F_{\alpha\beta}(\boldsymbol{r}) = (F_{LL}(r) - F_{NN}(r))\frac{r_\alpha r_\beta}{r^2} + F_{NN}(r)\delta_{\alpha\beta},$$

F_{LL} and F_{NN} are respectively the longitudinal and the lateral force correlations [34]. The inverse Fourier transform of $\hat{F}(k)$ gives

$$F_{LL}(r) = \frac{2\varepsilon}{3\ln(k_d/k_o)}\left[\frac{\cos(k_d r) r k_d - \sin(k_d r) r^2 k_d^2 - \sin(k_d r) + \mathrm{ci}(k_d r) r^3 k_d^3}{r^3 k_d^3} - \frac{\cos(k_o r) r k_o - \sin(k_o r) r^2 k_o^2 - \sin(k_o r) + \mathrm{ci}(k_o r) r^3 k_o^3}{r^3 k_o^3}\right], \tag{12}$$

and

$$F_{NN}(r) = \frac{\varepsilon}{3\ln(k_d/k_o) r^3 k_d^3 k_o^3}\left[k_o^3 \sin(k_d r) + k_d^3 \cos(k_o r) r k_o + 2k_d^3 \sin(k_o r) r^2 k_o^2 + 2k_o^3 \mathrm{ci}(k_d r) r^3 k_d^3 - k_d^3 \sin(k_o r) - k_o^3 \cos(k_d r) r k_d - 2k_o^3 \sin(k_d r) r^2 k_d^2 - 2k_d^3 \mathrm{ci}(k_o r) r^3 k_o^3\right].$$

Figure 1(b) shows F_{LL} and F_{NN} for $k_o = 1$, $k_d = 120$, and $\varepsilon = 0.15$ which are approximately the values used for the simulations (see Subsection 5.2). The amplitudes of F_{LL} and F_{NN} do not exceed a few percent of $F_{LL}(0)$ and $F_{NN}(0)$ in the interval $[\pi, 2\pi]$. Therefore the restriction of the domain to a periodic cubic box of volume $(2\pi)^3$ is valid.

The remark of the last paragraph, Subsection 2.1, applies also to the Navier–Stokes problem. In particular the correlation function of the forcing, when $k_o \to 0$ while ε is kept constant, is

$$F_{\alpha\beta}(\boldsymbol{r}) = \frac{2\varepsilon}{3}\delta_{\alpha\beta}.$$

The turbulence driven by this random forcing has been introduced by Novikov [1] and is referred to as Novikov's turbulence. Like for the Burgers problem, an external length scale λ_f characteristic of the forcing may be defined as

$$\lambda_f = \left(-\frac{F_{\alpha\alpha}(0)}{2F''_{\beta\beta}(0)}\right)^{1/2}.$$

It is easy to show that when $k_o \to 0$, $\lambda_f \to \infty$.

3. A RUNGE–KUTTA SCHEME FOR ADDITIVE NOISE PROBLEMS

In this section we derive a second-order Runge–Kutta scheme for the numerical integration of an equation of the type

$$d\boldsymbol{y}(t) = \boldsymbol{a}(t, \boldsymbol{y}(t))\, dt + B(t)\, d\boldsymbol{w}(t), \tag{13}$$

where $\boldsymbol{y}(t)$, $\boldsymbol{a}(t, \boldsymbol{y}(t))$ are M-dimensional vector valued functions, $B(t)$ is a $M \times M$ matrix valued function, and $\boldsymbol{w}(t)$ is a M-dimensional standard Wiener process. This equation may represent either the Burgers or the Navier–Stokes equations discretized in space. For instance, let us consider Eq. (3). We define $\{k_m \mid m = 1, \ldots, M\}$ the discrete set of wave numbers. The vector $\boldsymbol{y}$ is defined by

$$y_m(t) = \hat{v}(k_m, t)\exp\left(\nu k_m^2 t\right).$$

The reader will note that we use the integrating factor $\exp(\nu k_m^2 t)$ to eliminate the linear viscous term in the equation. The function $\boldsymbol{a}(\cdot, \cdot)$ is the nonlinear term

$$a_m(\boldsymbol{y}(t), t) = -\frac{ik_m \exp\left(\nu k_m^2 t\right)}{2} \sum_{k_p + k_q = k_m} \hat{v}(k_p, t)\hat{v}(k_q, t),$$

while the matrix $B(t)$ is defined by the relation

$$B_{mp}(t)dw_p(t) = f(k_m, t)\exp\left(\nu k_m^2 t\right),$$

where $f(k_m, t)$ is the stochastic forcing defined by Eqs. (5) and (6).

For the sake of completeness, we shall present the Ito formula and the notion of weak convergence related to the numerical approximation of stochastic differential equations. More precisely, the usual Taylor expansion, used to demonstrate the consistency of classical integration schemes can be extended to stochastic differential equations by iterated applications of the Ito formula to form the Ito-Taylor series. Then, the series is truncated according to the order and the type of convergence (weak in our case) required. A complete presentation on the numerical approximations of stochastic differential equations is provided in Kloeden and Platen [32].

The problem is to build, from a vector $\boldsymbol{y}(t)$, an approximation of $\boldsymbol{y}(t+\Delta t)$ where Δt is the time step. One can always write

$$\boldsymbol{y}(t+\Delta t) = \boldsymbol{y}(t) + \int_t^{t+\Delta t} \boldsymbol{a}(s, \boldsymbol{y}(s))\, ds + \int_t^{t+\Delta t} B(s)\, d\boldsymbol{w}(s), \tag{14}$$

where the second integral is the Ito integral. To expand the increments of smooth functions of Ito processes (such as $\int \boldsymbol{a}(s, \boldsymbol{y}(s))\, ds$) in the construction of numerical methods, it is advantageous to have a stochastic expansion formula with analogous properties to the deterministic Taylor formula. Such expansion may be obtained by iterated application of the Ito formula and is called the Ito–Taylor expansion. We recall the Ito formula [32] for an arbitrary function $\boldsymbol{c}(s, \boldsymbol{y}(s))$ of the solution $\boldsymbol{y}(s)$ of Eq. (13) (we take $s > t$)

$$\begin{aligned} &c_l(s, \boldsymbol{y}(s)) \\ &\quad = c_l(t, \boldsymbol{y}(t)) + \int_t^s \partial_i c_l(\sigma, \boldsymbol{y}(\sigma)) B_{ij}(\sigma)\, dw_j(\sigma) + \int_t^s \partial_i c_l(\sigma, \boldsymbol{y}(\sigma)) a_i(\sigma, \boldsymbol{y}(\sigma))\, d\sigma \\ &\qquad + \frac{1}{2} \int_t^s \partial_i \partial_k c_l(\sigma, \boldsymbol{y}(\sigma)) B_{ij}(\sigma) B_{kj}(\sigma)\, d\sigma + \int_t^s \partial_t c_l(\sigma, \boldsymbol{y}(\sigma))\, d\sigma. \end{aligned} \tag{15}$$

The notations ∂_i and ∂_t represent the partial derivatives $\partial/\partial x_i$ and $\partial/\partial t$, respectively. We apply this formula recursively to expand the function $\boldsymbol{a}(s, \boldsymbol{y}(s))$ in Eq. (14). The simplest nontrivial Ito–Taylor expansion is given in the Appendix as an illustration. To order the terms of the expansion, we introduce the following notation. We define a multi-index $\boldsymbol{\alpha} = (\alpha_1, \ldots, \alpha_\Lambda)$ such that $\alpha_i \in \{0, 1, \ldots, M\}$; $\Lambda(\boldsymbol{\alpha}) = \Lambda$ is the length of the multi-index. We write $\boldsymbol{\alpha}^-$ for the multi-index obtained by deleting the last component. Then we define the multiple Ito integral $I_{\boldsymbol{\alpha}}[c(\cdot)]_{t,s}$ of an arbitrary function $c(t)$ recursively by

$$I_{\boldsymbol{\alpha}}[c(\cdot)]_{t,s} = \begin{cases} c(s) & \text{if } \Lambda = 0, \\ \int_t^s I_{\boldsymbol{\alpha}^-}[c(\cdot)]_{t,\sigma}\, d\sigma & \text{if } \Lambda \geq 1 \text{ and } \alpha_\Lambda = 0, \\ \int_t^s I_{\boldsymbol{\alpha}^-}[c(\cdot)]_{t,\sigma}\, dw_{\alpha_\Lambda}(\sigma) & \text{if } \Lambda \geq 1 \text{ and } \alpha_\Lambda \geq 1. \end{cases}$$

The Ito–Taylor expansion of $\boldsymbol{y}(t+\Delta t)$ may be written in the general form

$$\boldsymbol{y}(t+\Delta t) = \sum_{\boldsymbol{\alpha}} I_{\boldsymbol{\alpha}}[\mathcal{C}_{\boldsymbol{\alpha}}(t, \boldsymbol{y}(t))]_{t,t+\Delta t}, \tag{16}$$

where the functions $\mathcal{C}_{\boldsymbol{\alpha}}(\cdot, \cdot)$ are called Ito coefficient functions. Following Proposition 1 (see Appendix), we drop the integrals such that $\Lambda(\boldsymbol{\alpha}) > 2$. We find

$$\begin{aligned} \tilde{y}_l(t+\Delta t) = y_l(t) &+ \int_t^{t+\Delta t} B_{lj}(s)\, dw_j(s) + a_l(t, \boldsymbol{y}(t))\Delta t + \partial_t a_l(t, \boldsymbol{y}(t)) \frac{\Delta t^2}{2} \\ &+ \partial_i a_l(t, \boldsymbol{y}(t)) \int_t^{t+\Delta t} \int_t^s B_{ij}(\sigma)\, dw_j(\sigma)\, ds \\ &+ \frac{1}{2} \partial_i \partial_k a_l(t, \boldsymbol{y}(t)) \int_t^{t+\Delta t} \int_t^s B_{ij}(\sigma) B_{kj}(s)\, d\sigma\, ds \\ &+ \partial_i a_l(t, \boldsymbol{y}(t)) a_i(t, \boldsymbol{y}(t)) \frac{\Delta t^2}{2}. \end{aligned} \tag{17}$$

The approximation is consistent to second-order in the weak sense,

$$|\langle g(\boldsymbol{y}(t+\Delta t))\rangle - \langle g(\tilde{\boldsymbol{y}}(t+\Delta t))\rangle| = O(\Delta t^3),$$

where $g(y)$ is any real-valued function six times continuously differentiable for which $g(y)$ and all its partial derivatives of order up to and including six have polynomial growth. Essentially, the weak order of convergence yields the rate of convergence of all the polynomial-form statistics of the approximate solution towards the same statistics of the true solution. Therefore, weak convergence is adequate for many applications including ours.

Using the Taylor expansion of $B(s)$ in Eq. (17), we can write

$$\begin{aligned} y_l(t+\Delta t) = y_l(t) &+ B_{lj}(t) I_j^{(1)} + a_l(t,\boldsymbol{y}(t))\Delta t + \partial_t B_{lj}(t) I_j^{(2)} \\ &+ \partial_i a_l(t,\boldsymbol{y}(t)) B_{ij}(t) I_j^{(3)} + \frac{1}{4}\partial_i\partial_k a_l(t,\boldsymbol{y}(t)) B_{ij}(t) B_{kj}(t)\Delta t^2 \\ &+ \frac{1}{2}\partial_i a_l(t,\boldsymbol{y}(t)) a_i(t,\boldsymbol{y}(t))\Delta t^2 + \frac{1}{2}\partial_t a_l(t,\boldsymbol{y}(t))\Delta t^2 + O(\Delta t^3), \end{aligned}$$

where the integrals are given by

$$I_j^{(1)} = \int_t^{t+\Delta t} dw_j(s), \qquad I_j^{(2)} = \int_t^{t+\Delta t}\int_t^s d\sigma\, dw_j(s),$$

$$I_j^{(3)} = \int_t^{t+\Delta t}\int_t^s dw_j(\sigma)\, ds.$$

Now we have to focus on evaluating consistently the integrals $I_j^{(1)}$, $I_j^{(2)}$, and $I_j^{(3)}$. According to formula (5.12.9) in [32], we approximate $I_j^{(1)} \approx \xi_j \Delta t^{1/2}$ and $I_j^{(2)} \approx I_j^{(3)} \approx \Delta t^{3/2}\xi_j/2$ where ξ_j is a standard Gaussian random variable.

Finally, we propose the approximation

$$\begin{aligned} \bar{y}_l(t+\Delta t) &= y_l(t) + \frac{1}{2}\left(\kappa_l^{(1)}(t) + \kappa_l^{(2)}(t)\right), \\ \kappa_l^{(1)}(t) &= a_l(t,\boldsymbol{y}(t))\Delta t + B_{lj}(t)\xi_j \Delta t^{1/2}, \\ \kappa_l^{(2)}(t) &= a_l\left(t+\Delta t, \boldsymbol{y}(t) + \boldsymbol{\kappa}^{(1)}(t)\right)\Delta t + B_{lj}(t+\Delta t)\xi_j \Delta t^{1/2}. \end{aligned}$$

It is easy to show, using the Taylor expansions of $\boldsymbol{a}(t+\Delta t, \boldsymbol{y}(t) + \boldsymbol{\kappa}^{(1)}(t))$ and $B_{lj}(t+\Delta t)$ about t and $\boldsymbol{y}(t)$ and our previous calculation that this approximation is consistent to second-order except that we get

$$\frac{1}{4}\partial_i\partial_k a_l(t,\boldsymbol{y}(t)) B_{ij}(t)\xi_j B_{km}(t)\xi_m \Delta t^2,$$

instead of the term

$$\frac{1}{4}\partial_i\partial_k a_l(t,\boldsymbol{y}(t)) B_{ij}(t) B_{kj}(t)\Delta t^2.$$

But since, $\langle(\delta_{jm} - \xi_j\xi_m)^2\rangle = 0$, the above term does not modify the order of the approximation. When this approximation is used as an integration scheme for Eq. (13) supplemented

with an initial condition $\boldsymbol{y}(0) = \boldsymbol{y}_0$, and provided that this scheme is stable for the particular problem, after an arbitrary number of iterations, say n, it gives an approximate solution $\boldsymbol{y}^{(n)}$ which is such that $|\langle g(\boldsymbol{y}^{(n)})\rangle - \langle g(\boldsymbol{y}(n\Delta t))\rangle| = O(\Delta t^2)$. This scheme is the vectorial additive noise version of the Runge–Kutta scheme proposed by Petersen [35].

4. NUMERICAL METHODS

In this section, we present some details about the algorithms, their implementation, and their computational performances. After a few words about the stability of the temporal integration scheme in Subsection 4.1, we briefly recall, in Subsection 4.2, the random shifting procedure used to remove aliased interactions. The random number generator is discussed in Subsection 4.3. Finally, Subsection 4.4 gives the main important figures concerning the computational performance of the Navier–Stokes solver.

4.1. *Time Discretization*

The time discretization method is based on the second-order Runge–Kutta algorithm presented in Section 3. The linear diffusion term is treated with an integrating factor. Hereafter, we study the linear stability of this scheme in order to provide an estimate of the time step upper bound as a function of the maximum velocity v_{max}, the spatial resolution N (N is the number of modes of the Fourier expansion in one spatial direction), and the kinematic viscosity ν. The linear model-equation under consideration reads

$$\frac{dv}{dt}(t) = -\frac{i v_{max} N}{2} v(t) - \frac{\nu N^2}{4} v(t).$$

This equation represents the evolution of the amplitude of the velocity for the mode $N/2$ which is the worst case since it corresponds to the highest eigenvalue. For this equation, the integrating factor is $\exp(\nu N^2 t/4)$. Therefore we define

$$y(t) = v(t) \exp\bigl(\nu N^2 t/4\bigr),$$

and the equation for $y(t)$ is

$$\frac{dy}{dt}(t) = -\frac{i v_{max} N}{2} y(t).$$

The calculation of the amplification factor of the second-order Runge–Kutta scheme for this problem (in the limit of small Δt) leads to

$$|y^{n+1}| \le \exp\left(\frac{N^4 v_{max}^4 \Delta t^4}{128}\right) |y^n|,$$

where Δt is the time step and y^n is the approximation of $y(n\Delta t)$. Going back to the original problem, we have now

$$|v^{n+1}| \le \exp\left(\frac{N^4 v_{max}^4 \Delta t^4}{128} - \frac{\nu N^2 \Delta t}{4}\right) |v^n|,$$

which gives the stability condition

$$\Delta t \leq (32)^{1/3}\left(\frac{\nu}{v_{max}^4 N^2}\right)^{1/3}.$$

If an hyperviscosity is used, the condition becomes

$$\Delta t \leq \left(\frac{128}{2^{2h}}\right)^{1/3}\left(\frac{\nu_h N^{2h-4}}{v_{max}^4}\right)^{1/3}.$$

For comparison, if, instead of the second-order Runge–Kutta scheme, we use a second-order Adams–Bashforth method, the condition is

$$\Delta t \leq (16)^{1/3}\left(\frac{\nu}{v_{max}^4 N^2}\right)^{1/3}.$$

Since the Runge–Kutta method requires two evaluations of the nonlinear terms per time step while the Adams–Bashforth algorithm needs only one, it seems more advantageous to use the Adams–Bashforth scheme. Nonetheless, as we will show in the next paragraph, the dealiasing can be achieved at no extra cost for the Runge–Kutta scheme by using a random shifting method, while for the Adams–Bashforth technique the standard shifting method requires an extra evaluation of the nonlinear terms per time step.

Finally, the reader may raise the question: Does the stochastic term influence the numerical stability properties of the scheme? In our case, we can show easily that the amplification factor is the same as the one for the corresponding deterministic equation. Consequently, the linear stability constraint of the deterministic problem is also valid for the stochastic one.

4.2. *Spatial Discretization*

In a simulation of homogeneous turbulence, the spatial resolution is chosen accordingly to the characteristic length scale of the dissipative subrange (defined as the scales of motion for which the viscous effects are dominant):

$$l_v = \left(\frac{\nu^3}{\varepsilon}\right)^{1/4}.$$

This length scale is referred to as the Kolmogorov length scale. With a resolution such that $k_d \approx k_v = 1/l_v$ we expect to have a good representation of the inertial subrange scales. If a hyperviscous dissipation is used instead of the normal viscosity, the Kolmogorov length scale is defined by

$$l_v = \left(\frac{\nu_h^3}{\varepsilon}\right)^{\frac{1}{6h-2}}. \tag{18}$$

The spatial discretization method is the Fourier spectral method (Canuto *et al.* [28]). The nonlinear terms are evaluated by a pseudospectral procedure. The aliasing errors are reduced by the random shifting technique suggested by Rogallo [36]. Since the time differencing scheme is a second-order Runge–Kutta, at each time step we have two evaluations of a

convolution product of the form

$$\hat{w}_k = \sum_{m+n=k} \hat{u}_m \hat{v}_n.$$

Instead of evaluating this product by the standard pseudospectral algorithm, one introduces a phase shift Δ in the discrete Fourier transform:

$$u'_j = \sum_{k=-N/2}^{N/2-1} \hat{u}_k e^{ik(2\pi j/N+\Delta)}, \qquad v'_j = \sum_{k=-N/2}^{N/2-1} \hat{v}_k e^{ik(2\pi j/N+\Delta)},$$

$$\hat{w}'_k = \frac{1}{N} \sum_{j=0}^{N-1} u'_j v'_j e^{-ik(2\pi j/N+\Delta)}.$$

At the first stage of the Runge–Kutta algorithm, we take $\Delta = \Delta_1 = 2\pi u/N$, with u a random variable uniformly distributed on the interval [0, 1[. For the second stage, we fix $\Delta = \Delta_1 + \pi/N$. As a result, the aliasing error is reduced, at the end of one Runge–Kutta step, by a factor of the order $O(\Delta t^2)$ compared to the pure pseudospectral aliasing error. The random variable in the definition of the phase shift ensures that the aliasing errors are uncorrelated from step to step. For three-dimensional problems, the random shifting method reduces the singly aliased interactions. The doubly and triply aliased interactions are dropped by the spherical truncation of modes

$$k_1^2 + k_2^2 + k_3^2 > k_{max}^2 = \frac{2N^2}{9}. \tag{19}$$

4.3. *The Stochastic Forcing*

In this section we address the problem of choosing an appropriate method to generate pseudorandom numbers for the construction of the stochastic forcing. Due to the resolution we want to achieve for the stochastic Navier–Stokes problem ($N^3 = 256^3$) two fundamental properties are required. Firstly, the generator should be able to produce huge sequences of independent random numbers: at each time step, we have to compute three arrays of 256^3 random numbers and, since the number of time steps for a typical simulation is 50,000, the period of the random number generator must be greater than 2.517×10^{12}. Secondly, since we generate 256^3 random numbers per time step, the computational performance of the generator is also a critical issue and has to be optimal on a vector computer which is the machine architecture we use.

A survey of the theory and the more common techniques for testing a uniformly distributed random number generator may be found in Knuth [37]. A more recent review of the usual generators with a discussion about the implementation of random number generators on vector computers is given by Anderson [29]. The most common method to generate random numbers is the linear congruential generator. As an example of such kind of generator, we consider the so-called GGL generator [38] given by the formula $x_n = (16807 \times x_{x-1}) \bmod(2^{31} - 1)$. This generator has a full period $p = 2^{31} - 1 \approx 2.147 \times 10^9$ which is too short for our problem. Moreover, the algorithm is sequential and cannot be efficiently implemented on a vector computer. In order to show the importance of the period, we have performed a Navier–Stokes simulation with a short period generator. Clearly, one can see the repetition of the same pattern in the evolution of kinetic energy reported in Fig 2. The

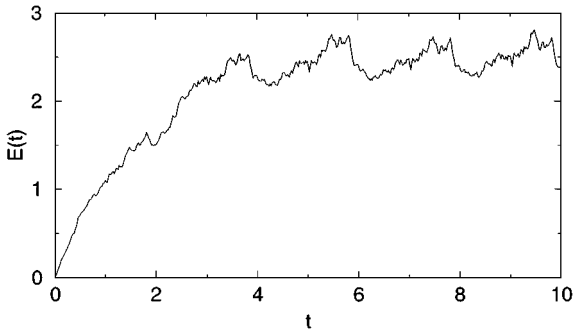

FIG. 2. Time evolution of the kinetic energy $E(t)$ for a randomly forced Navier–Stokes simulation with a short period random number generator.

resolution of the simulation is $N^3 = 128^3$ and the period of the random number generator is $p \approx 2.097 \times 10^9$.

Instead of linear congruential generator, we use an algorithm based on lagged Fibonacci series:

$$t = x_{n-p} + x_{n-q},$$
$$x_n = t - \text{float}(\text{int}(t)).$$

This generator has been implemented by Petersen [30, 31] on the NEC SX-3 and SX-4 with the lags $(p, q) = (273, 607)$ chosen on the basis of performance (NEC computers have a vector length of $L = 256$) and because this method generates a sequence of very long period ($p \approx 10^{191}$ on 32-bit mantissa computers). About the quality of the random sequence, the generator went successfully through a suite of tests performed by Petersen [31]. Finally, we notice that the lagged Fibonacci series has to be initialized by a sequence of 607 random numbers. We have used the GGL generator presented above as an initializer with the seed $s = 667790$ (this generator has also been tested extensively).

4.4. *Computational Performances of the Navier–Stokes Solver*

The Navier–Stokes program was run on two different NEC computers in the following configurations: (i) the NEC SX-3 for which one vector unit has a peak performance of 6.4 Gflops and a maximum available memory of 1 Gbyte; (ii) the NEC SX-4 with a maximum available memory for a job running on a single processor of 1.5 Gbytes and a single processor peak performance of 2 Gflops. The main memory of these two computers is supplemented by an eXtended Memory Unit (XMU). The maximum resolution one can achieve is constrained by the memory requirements of the algorithm. Each scalar field is stored in one array. The Runge–Kutta scheme implemented for the Navier–Stokes problem needs at least eight arrays (the Runge–Kutta algorithm needs at least three vector fields, therefore, in three dimensions nine scalar fields are required; however, one of them can be eliminated using the incompressibility constraint), to which we have to add two extra arrays to store the stochastic forcing (again, the third component of the forcing is not required by virtue of the incompressibility constraint). All of the figures we give in this paragraph are relative to a typical 256^3 run on one processor. For that resolution, one array requires 128 Mbytes. Therefore we keep six arrays in the main memory while the other four arrays are sent to the XMU. The computational performance of the solver is 1.5 Gflops on the NEC SX-3 and

1 Gflops on the NEC SX-4. One time step iteration consumes 14.7 s on the NEC SX-3 and 20.5 s on the NEC SX-4. The time step is $\Delta t = 10^{-3}$ (for the normal Laplacian dissipation) and the turnover time is $\tau_E \approx 2.02$. Therefore a complete turnover time takes approximately 8.2 h on the NEC SX-3 and 11.5 h on the NEC SX-4.

5. RESULTS

This section is devoted to the presentation the numerical results obtained for the stochastic Burgers and Navier–Stokes problems defined in Section 2. For both problems, the third-order structure functions are compared with their exact expressions in the inertial subrange. For the Burgers equation with a normal Laplacian diffusive term ($h = 1$), we reproduce some of the results obtained by Chekhlov and Yakhot [22, 23]. The agreement is very good though, in their work, they have used hyperviscosity ($h = 6$) to broaden the inertial subrange. An interesting conclusion is that, contrary to the system treated by Leveque and She [15], the statistical properties of the inertial subrange of the Burgers problem is independent of the dissipation mechanism. We also computed temporal structure functions. Our results show that random sweeping is the dominant effect, i.e., the so-called random Taylor hypothesis is valid for this system. Concerning the Navier–Stokes simulations, we have performed two calculations: one with a normal Laplacian dissipation and another one with a hyperviscous dissipation. The energy spectra present some remarkable differences even if the probability density functions of the velocity increments for the two simulations are almost identical in the inertial subrange. Finally, we show that, for this problem, the Eulerian energy frequency spectrum agrees also with the random Taylor hypothesis.

Before starting, we shall comment on the averaging methods we use in practice and their connection with the ensemble average used in the theoretical discussion. The estimation of statistical quantities is a central question in the theory of stochastic processes. The main concept is the one of ergodicity: a time (resp. space) ergodic random function is such that the time average (resp. volume average) of a given instantaneous quantity converges towards the ensemble average of that quantity as the time interval (resp. volume) on which the average is taken goes to infinity. An obvious necessary condition for this property is that the random function should be stationary (resp. homogeneous). The problems described in Section 2 are homogeneous since the domain and the forcing are taken to be homogeneous. Moreover, the solutions are assumed to reach a statistical steady state after a finite time t^*. However, this condition is not sufficient. An example of a sufficient condition is given by the Slutsky's theorem (see, e.g., Papoulis [39]): a stationary random function $a(t)$ which is such that its autocorrelation function $R(\tau) = \langle a(t+\tau)a(t)\rangle$ satisfies

$$\frac{1}{T}\int_0^T R(\tau)\,d\tau \to 0, \qquad \text{when } T \to \infty,$$

is mean ergodic (the time average of $a(t)$ is an unbiased estimator of the mean of $a(t)$). A similar theorem holds for volume average of homogeneous random functions.

In practice, ergodicity will be assumed. Most of our statistics are spatial averaged or shell averaged estimators (i.e., we average on a shell of wave-numbers in spectral space for multi-dimensional problems). When it is possible, time averages are used in addition to improve the estimation. The integral of the time average is discretized with a time step of the order of the decorrelation time of the velocity autocorrelation (turnover time) so that it resembles an ensemble average between weakly correlated realizations.

TABLE I
Parameters of the Stochastic Burgers Calculation

N	Δt	T	ν	E	ε	k_o	k_d
32768	5×10^{-6}	8.1575	1×10^{-5}	1.680	8.660	1	16384

5.1. *Burgers*

The parameters of the simulation are reported in Table I where N is the number of modes, Δt is the time step, T is the total time of integration, ν is the kinematic viscosity, E and ε are respectively the mean kinetic energy and the mean dissipation rate, and k_o and k_d are the infrared and the ultraviolet cutoffs. Figure 3 shows the time evolution of the space averaged kinetic energy $E(t)$ and dissipation rate $\varepsilon(t)$ (E and ε in Table I are the time averages of $E(t)$ and $\varepsilon(t)$, respectively). From Fig. 3, we can fix $t^* = 1$ such that, for $t > t^*$, the flow is considered to be statistically stationary. Even if the quantities are averaged on the spatial domain, they remain very fluctuating. The time scale of the largest fluctuations of $E(t)$ are of the order of $T/16$, therefore we expect bad time averaged estimations of quantities relative to the large-scale dynamics. Nevertheless, most of the statistics estimated in the following are relative to the intermediate-scale dynamics (the inertial subrange) for which the sample is large enough. A detailed inspection of Fig. 3 shows some coherence between the fluctuations of energy and dissipation rate. For instance, the "burst" $1 < t < 1.5$ in Fig. 3 (a) is followed by the narrower event at time $t \approx 1.5$ in graph (b); the same kind of behavior, in the direction of a weaker amplitude, is observed for $7 < t < 7.5$ for the energy and $t \approx 7.4$ for the dissipation rate.

The instantaneous velocity field at time $t = 4$ is represented on Fig. 4. The solution consists in a set of randomly distributed backward pseudoshocks. Recall that due to the viscous term present in the equation, the solution remains smooth. In the literature these "smooth" singularities are sometimes referred to as near singularities or pseudoshocks. Magnifications of the solution, given by Figs. 4(b) and 4(c), illustrate the structure of the solution. The shocks

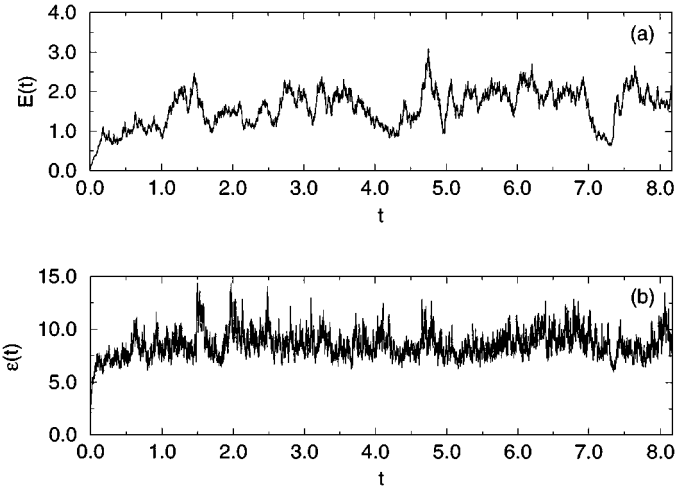

FIG. 3. Time evolution of the kinetic energy $E(t)$ and the dissipation rate $\varepsilon(t)$.

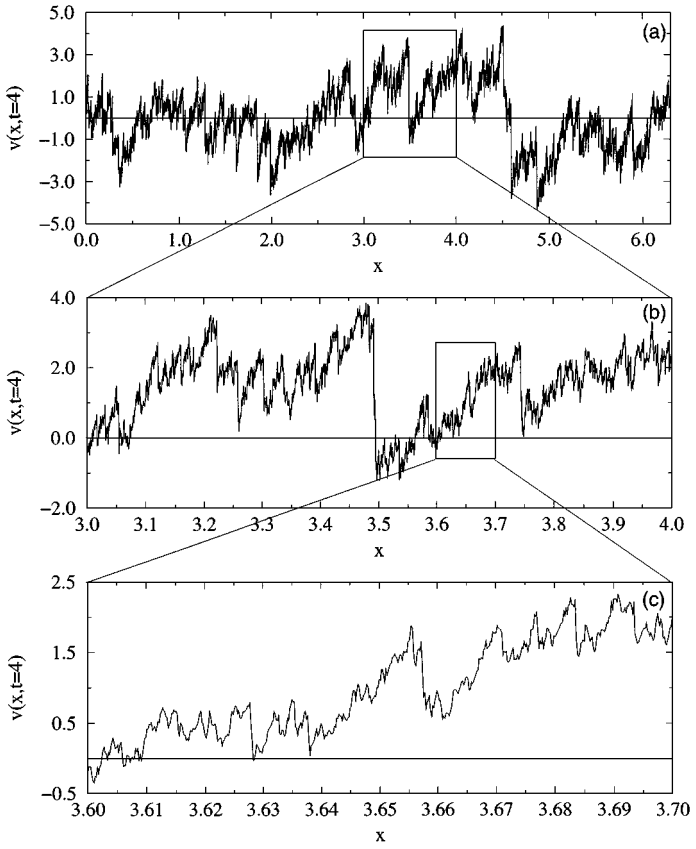

FIG. 4. Solution $v(x, t)$ of the stochastic Burgers problem at time $t = 4$. The magnifications illustrate the structure of the solution.

are present in many scales (the amplitude of a shock defines its scale). The smallest ones are clearly smoothed by the viscous diffusion. The large-scale shocks are very persistent structures and they move with a small velocity which is the difference between the velocities of the shock edges. Figure 5 shows the evolution of a region near a strong shock (in the

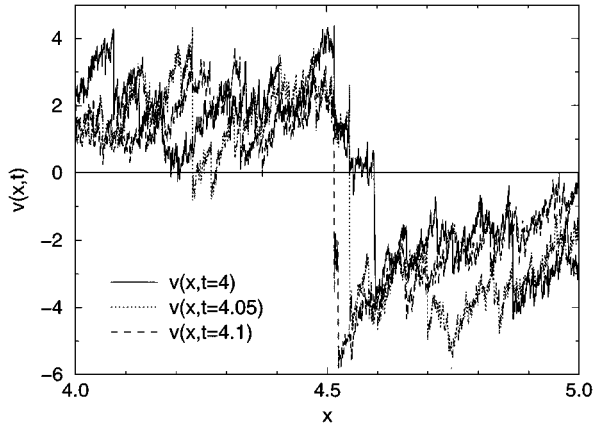

FIG. 5. Time evolution of the solution $v(x, t)$ of the stochastic Burgers problem near a strong shock.

middle of the figure) by giving the velocity field at three different times. The small-scales fluctuate strongly during this time interval while the large-scale shock does not evolve very much. (Note that between $t = 4$ and $t = 4.1$ there are 10,000 time steps.)

The energy spectrum is defined by

$$E(k) = \frac{1}{2}\left\langle |\hat{v}_k|^2 + |\hat{v}_{-k}|^2 \right\rangle;$$

here the symbol $\langle \cdot \rangle$ denotes the time average. The energy flux reads

$$\Pi(k) = \sum_{k<p<\infty} T(p), \tag{20}$$

where $T(k)$ is the energy transfer, given by

$$T(k) = \langle \hat{v}_k \hat{w}_k + \hat{v}_{-k} \hat{w}_{-k} \rangle, \qquad \text{with } \hat{w}_k = ik \sum_{m+n=k} \hat{v}_m \hat{v}_n.$$

The energy transfer appears in the energy equation

$$\hat{F}(k) + T(k) = 2\nu k^2 E(k), \tag{21}$$

where $\hat{F}(k)$ is the energy injection spectrum defined in Section 2, Eq. (6). The energy flux $\Pi(k)$ is the rate of energy transferred by all modes $|p| < k$ to modes $|p| > k$. The energy spectrum $E(k)$ and the rescaled energy flux $\Pi(k)/\ln(k)$ are represented on Figs. 6(a) and 6(b). The graph shows clearly a subrange of wave-numbers characterized by a energy spectrum $E(k) \propto k^{-5/3}$ and a flux $\Pi(k) \propto \ln(k)$. If we recall that $\hat{F}(k) \propto k^{-1}$, this particular energy flux is readily obtained from Eq. (21) by neglecting the viscous term. This region of the spectrum, where the dynamics is dominated by nonlinear effects, is referred to as the inertial subrange.

It is also interesting to characterize the inertial region in physical space. Let us denote the velocity increments by $\delta v(x, z) = v(x + z, t) - v(x, t)$. We define the structure functions $S_n(z)$ for all integer n,

$$S_n(z) = (-1)^n \langle (\delta v(x, z))^n \rangle.$$

On can find an exact expression for $S_3(z)$ provided that we take the size of the domain $L \to \infty$ and the kinematic viscosity $\nu \to 0$. The equation is

$$S_3(z) = 6 \int_0^z F(r)\, dr, \tag{22}$$

where $F(r)$ has been defined in Section 2, Eq. (7). Note that if $k_o \to 0$, Eq. (22) becomes $S_3(z) = 12\varepsilon z$, which is the Burgers equivalent for the Kolmogorov 4/5-law. By comparing this exact relation with $S_3(z)$ computed from the simulation, we can define a region where the agreement is good. In this inertial region, the dynamics is independent of the viscosity and of the size of the domain. Figure 7 gives $S_n(z)$ for $n = 3, 4, 5, 6, 7$ (dotted lines). For $n = 3$, the solid line is the theoretical prediction when $L \to \infty$ and $\nu \to 0$. We observe that for $n = 4, 5, 6, 7$, $S_n(z) \propto z^{\zeta_n}$ with $\zeta_n = 0.950 \pm 0.07$. These exponents are due to the

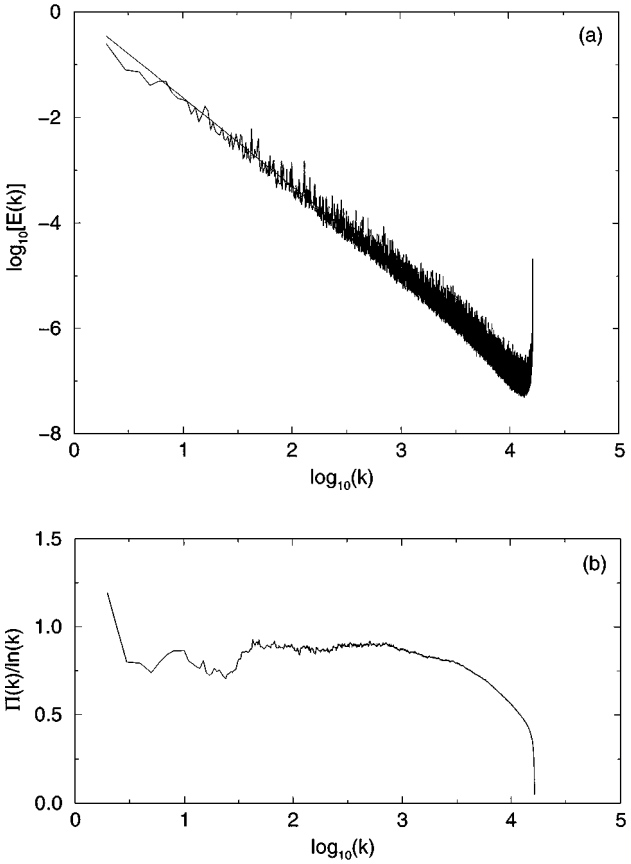

FIG. 6. (a) Energy spectrum $E(k)$—the straight line is the linear least-squares fit of the spectrum in the inertial subrange, its slope is -1.663 ± 0.007—and (b) compensated spectral energy flux $\Pi(k)/\ln(k)$.

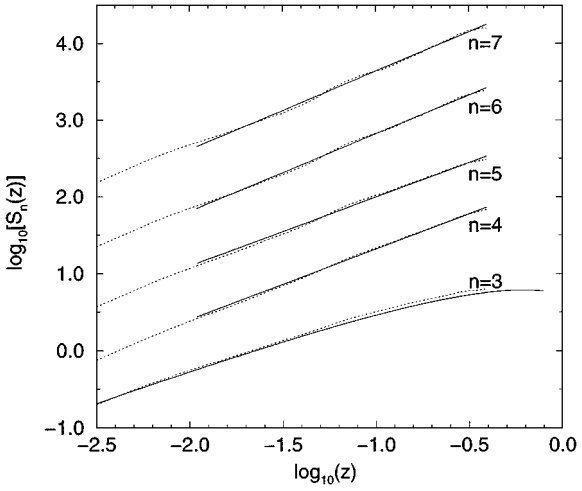

FIG. 7. Structure functions $S_n(z)$, for $n = 3, 4, \ldots, 7$ (dotted lines). For $n = 3$ (resp. $n > 3$), the solid line is the theoretical prediction (resp. the least-squares fits). The slope of the linear least-squares fits from $n = 4$ to $n = 7$: 0.913 ± 0.002, 0.895 ± 0.004, 1.010 ± 0.003, 1.025 ± 0.003.

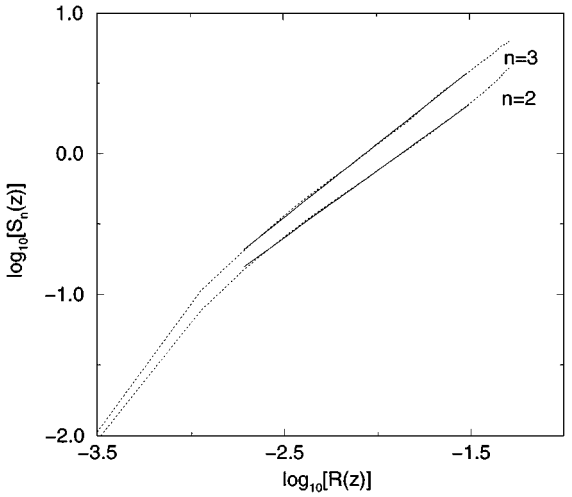

FIG. 8. Structure functions $S_n(z)$, for $n = 2, 3$, against $R(z)$ (dotted lines) and their linear least-squares fits (solid lines). Slope of the linear least-squares fits for $n = 2, 3$: 0.950 ± 0.002, 1.043 ± 0.003.

presence of strong shocks (Chekhlov and Yakhot [23]). If we define

$$R(z) = \frac{1}{2\varepsilon} \int_o^z F(r)\, dr,$$

we can write $S_3(z) = 12\varepsilon R(z)$. Then, if we plot $S_2(z)$ against $R(z)$ (Fig. 8), we find that $S_2(z) \propto R(z)^{\zeta_2}$ where $\zeta_2 = 0.950 \pm 0.002$. The results of the measurements of the structure functions $S_\alpha(z) = \langle |v(x+z,t) - v(x,t)|^\alpha \rangle$ with noninteger exponents $\alpha = 1/3, 2/3, \ldots, 6/3$, presented in Fig. 9 are in good agreement with $S_\alpha(z) \propto z^{\alpha/3}$. The result obtained for $\alpha = 6/3$ is consistent with $S_2(z) \propto R(z)^{0.95}$ since, in the region of interest, we have approximately $R(z) \propto z^{0.7}$.

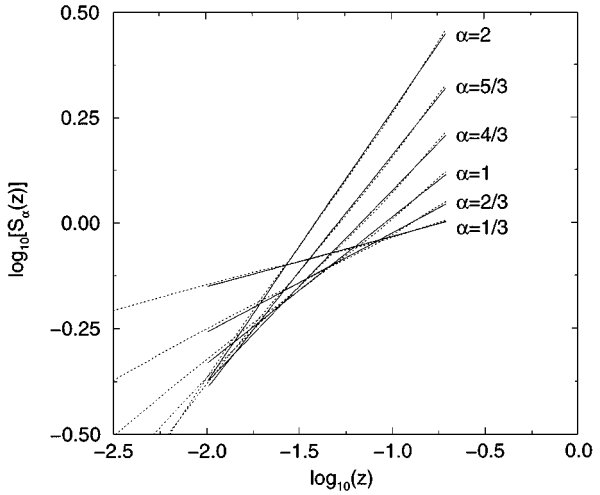

FIG. 9. Structure functions $S_\alpha(z)$, for noninteger exponents $\alpha = 1/3, 2/3, \ldots, 6/3$ (dotted curves). Slope of the linear least-squares fits (solid lines) from $\alpha = 1/3$ to $\alpha = 6/3$: 0.1186 ± 0.0005, 0.234 ± 0.001, 0.346 ± 0.001, 0.451 ± 0.001, 0.550 ± 0.001, 0.638 ± 0.001.

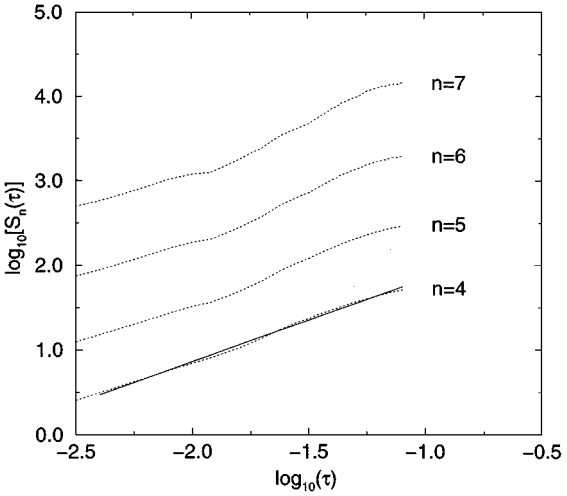

FIG. 10. Structure functions $S_n^t(\tau)$, for $n = 4, 5, 6, 7$ (dotted lines) and the linear least-squares fit for $n = 4$ (solid line, slope 0.97 ± 0.01).

There is also a region in the time domain where the time structure functions

$$S_\alpha^t(\tau) = \langle |v(x, t+\tau) - v(x, t)|^\alpha \rangle,$$

behave like $S_\alpha^t(\tau) \propto \tau^{\zeta_\alpha^t}$. Should $S_\alpha^t(\tau)$ be a function of τ and ε only, a simple dimensional argument leads to the following scaling prediction

$$S_\alpha^t(\tau) \propto (\varepsilon\tau)^{\alpha/2}. \tag{23}$$

Figures 10 and 11 show that this equation is not satisfied, which means that $S_\alpha^t(\tau)$ cannot be a function of τ and ε only. We will show that our results can be easily interpreted in the light

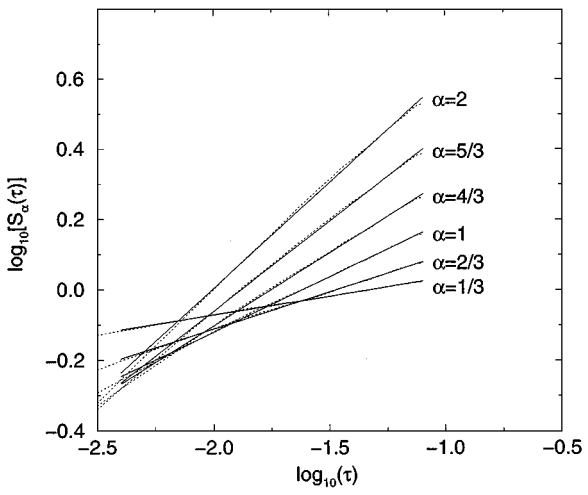

FIG. 11. Structure functions $S_\alpha^t(\tau)$, for noninteger exponents $\alpha = 1/3, 2/3, \ldots, 6/3$ (dotted curves). Slope of the linear least-squares fits (solid lines) from $\alpha = 1/3$ to $\alpha = 6/3$: 0.1066 ± 0.0005, 0.212 ± 0.001, 0.315 ± 0.001, 0.415 ± 0.002, 0.511 ± 0.003, 0.601 ± 0.004.

of the analysis of Tennekes [19], assuming that the sweeping of small-scales by the large-scales is the dominant interaction. From Fig. 4, we have observed that the number of large amplitude shocks is small compared to the number of smaller shocks. Large shocks can be considered as rare events. Moreover, we have seen on Fig. 5 that even if the large shocks are not evolving very fast, the small shocks move with a nonzero velocity. Consequently, we assume that, in the mean, the shocks are advected by a velocity field of magnitude $v_{rms} = \langle v(x,t)^2 \rangle^{1/2}$. We fix z in the inertial subrange and define $\tau = \text{sign}[v(x,t)]z/v_{rms}$. Then we write the following discrete inviscid Burgers equation:

$$\frac{v(x,t+\tau) - v(x,t)}{\tau} \approx -v(x,t)\frac{v(x+z,t) - v(x,t)}{z} + \frac{1}{\tau}\int_t^{t+\tau} f(x,\sigma)\, d\sigma. \quad (24)$$

Recall that the covariance of the last term in Eq. (24) is of the order $O(\tau^{-1})$. If we assume that the shocks are statistically independent of the background flow, we obtain for the mean square value of (24)

$$\frac{\langle (v(x,t+\tau) - v(x,t))^2 \rangle}{\tau^2} \approx v_{rms}^2 \frac{\langle (v(x+z,t) - v(x,t))^2 \rangle}{z^2} + \frac{F(0)}{\tau},$$

where $F(0) = 2\varepsilon$ (Novikov [1]). We now use the previous result

$$\langle (v(x+z,t) - v(x,t))^2 \rangle \approx \beta(\varepsilon z)^{2/3}, \qquad \beta > 0,$$

and we find that

$$S_2^t(\tau) \approx \beta v_{rms}^{2/3}(\varepsilon\tau)^{2/3} + 2\varepsilon\tau. \quad (25)$$

Figure 11 ($\alpha = 2$) shows that $S_2^t(\tau) \propto \tau^{0.6}$, indicating that the random sweeping (the first term of the right-hand-side of Eq. (25)) is the dominant effect. More generally, we have

$$S_\alpha^t(\tau) \propto S_\alpha(z) \qquad \text{with } z = v_{rms}\tau.$$

In Figs. 10 and 11, we observe that this relation is approximately correct since, in our calculation, $v_{rms} \approx 1.833$. This result is in contradiction with the conclusion of Chekhlov and Yakhot [22] and with the RG prediction (Yakhot *et al.* [18]) where it is argued that, in a randomly forced system such as the one we are studying, random sweeping does not contribute to the decorrelation.

5.2. *Navier–Stokes*

Two simulations have been performed for the following Navier–Stokes problem

$$\frac{\partial \boldsymbol{v}}{\partial t} + v_\beta \frac{\partial \boldsymbol{v}}{\partial x_\beta} = \boldsymbol{f} - \nabla p + (-1)^{h+1}\nu_h \nabla^{2h}\boldsymbol{v},$$
$$\nabla \cdot \boldsymbol{v} = 0,$$

where $\boldsymbol{f}(\boldsymbol{x}, t)$ is defined by the covariance given by Eq. (11), and ν_h is the hyperviscosity parameter. In the first simulation, $h = 1$ and the dissipative term is the usual Laplacian. For the second simulation, in order to increase the size of the inertial subrange, we have chosen

$h > 1$. Following the work of Borue and Orszag [13], we use $h = 8$. The coefficients ν_h and the dissipation rate ε are fixed so that the Kolmogorov wave-number $k_v = 1/l_v$ remains smaller than k_{max} (see the definition of l_v, Eq. (18), and k_{max}, Eq. (19)).

We recall here the definition of some characteristic quantities (see, e.g., Batchelor [40]) to be used in the following. The energy spectrum is given by

$$E(k) = \frac{1}{2} \sum_{k-1/2<|\boldsymbol{p}|\leq k+1/2} \langle |\hat{\boldsymbol{v}}(\boldsymbol{p}, t)|^2 \rangle,$$

for all integer $0 \leq k \leq k_d$. We define two length scales: the integral length scale

$$L = \frac{\sum_{k=0}^{k_d} k^{-1} E(k)}{\sum_{k=0}^{k_d} E(k)},$$

which is the distance over which there is an appreciable correlation between the values of the velocity field at two points, i.e., roughly speaking the size of the largest structures in the flow; the differential or Taylor microscale

$$\lambda = \left(\frac{\sum_{k=0}^{k_d} E(k)}{\sum_{k=0}^{k_d} k^2 E(k)} \right)^{1/2},$$

which is the curvature of the spatial velocity autocorrelations at the origin. The Taylor microscale is smaller than the integral scale and is related to the average of the scales belonging to the inertial subrange. The time scale associated to the integral scale is the eddy turnover time

$$\tau_E = L/v_{rms},$$

where v_{rms} is the root-mean-square velocity defined by $v_{rms} = (2E/3)^{1/2}$. Finally, s_3 and s_4 are, respectively, the velocity derivative skewness and flatness defined by the general relation

$$s_n = \frac{\langle (\partial v_1/\partial x_1)^n \rangle}{\langle (\partial v_1/\partial x_1)^2 \rangle^{n/2}}.$$

The main features of both simulations are reported in Tables II and III. The integral scale L remains much smaller than the half-size of the box and we expect limited finite size effects. The Taylor microscale λ is smaller in the hyperviscous case, which indicates that the inertial subrange is likely to be larger in that case. Our values for s_3 and s_4 are significantly smaller in absolute value compared to the results obtained by other authors [11, 12] for low wave-number forced turbulence.

Figure 12 represents the time evolution of the energy $E(t)$ and the dissipation rate $\varepsilon(t)$. These quantities are averaged in space. In the two simulations, the flow can be considered

TABLE II
Simulation Parameters of the Stochastic Navier–Stokes Calculations

	N	Δt	T	h	ν_h	k_o	k_d
Normal viscosity	256	10^{-3}	50	1	10^{-3}	1	120
Hyperviscosity	256	2×10^{-3}	60	8	1.38×10^{-30}	1	120

TABLE III
Flow Parameters of the Stochastic Navier–Stokes Calculations

	E	ε	L	λ	τ_E	s_3	s_4
Normal viscosity	0.415	0.159	1.062	0.162	2.023	−0.41	3.821
Hyperviscosity	0.42	0.16	0.956	0.092	1.807	−0.293	3.383

statistically stationary for times greater than $t^* = 10$. Observe that, contrary to large-scale forcing simulations, the evolution of $E(t)$ does not exhibit large-scale intermittency [14] (which is a typical effect of strong large-scale correlations due to the finite size domain).

The rate of energy transfer is given by the relation

$$T(k) = \sum_{k-1/2<|\boldsymbol{p}|\leq k+1/2} \langle \hat{\boldsymbol{v}}(\boldsymbol{p}) \cdot \boldsymbol{P}(\boldsymbol{p}) \widehat{(\boldsymbol{v} \times \boldsymbol{w})}(\boldsymbol{p}) \rangle,$$

where $\boldsymbol{w} = \boldsymbol{\nabla} \times \boldsymbol{v}$ is the vorticity and $\boldsymbol{P}(\boldsymbol{k})$ is the projector defined by Eq. (9). The hat over the velocity field $\boldsymbol{v}$ denotes here the discrete Fourier transform. The energy transfer appears in the energy equation

$$\mathcal{F}(k) + T(k) = 2\nu_h k^{2h} E(k),$$

where $\mathcal{F}(k) = 4\pi k^2 \hat{F}(k)$ with $\hat{F}(k)$ defined by Eq. (10). Like in the Burgers problem, Eq. (20) defines the energy flux $\Pi(k)$.

The energy spectrum $E(k)$ and the rescaled energy flux $\Pi(k)/\ln(k)$ are represented in Fig. 13. The viscous and hyperviscous spectra have a remarkable different shape. On one hand, the hyperviscous simulation shows a small power-law (inertial) region. If we examine the energy flux, we observe a narrow dissipative subrange (i.e., where the energy flux drops). However, the energy spectrum shows a "bump" which prevents the formation of a broad

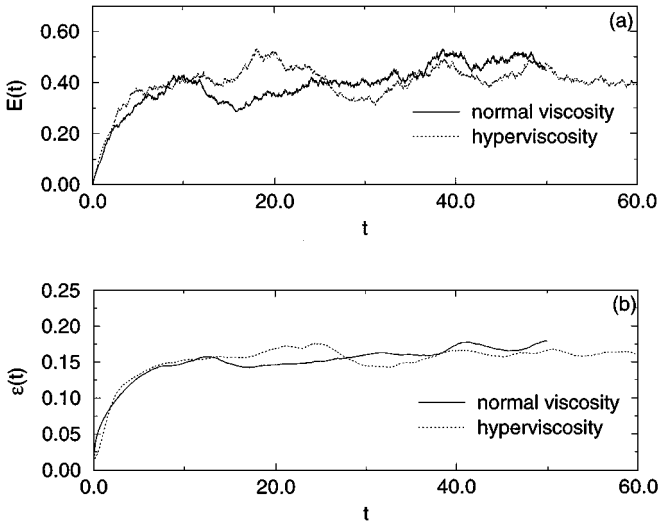

FIG. 12. Time evolution of the kinetic energy $E(t)$ (a) and the dissipation rate $\varepsilon(t)$ (b).

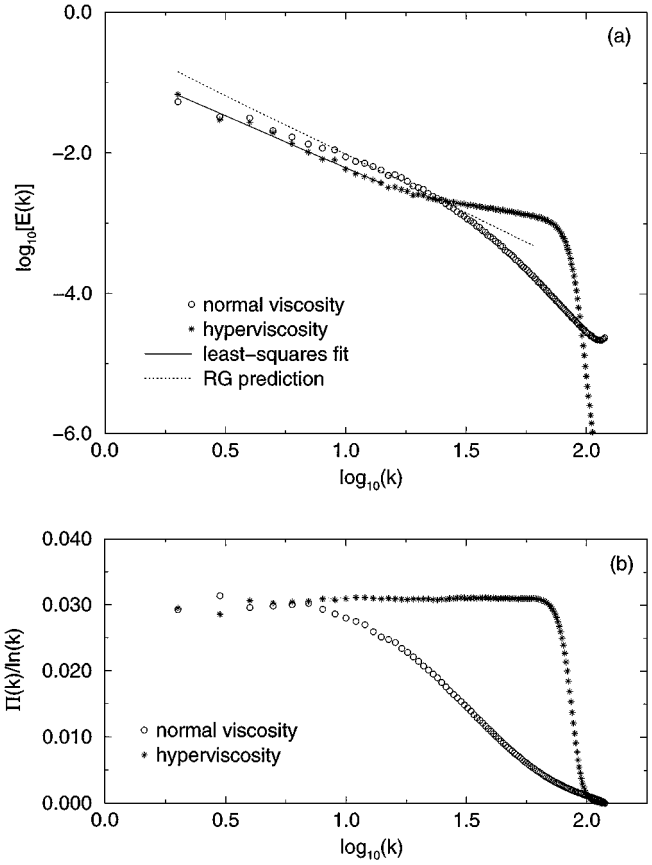

FIG. 13. Energy spectrum $E(k)$ (a) and compensated energy flux $\Pi(k)/\ln(k)$ (b). In graph (a), the solid line is the least-squares fit obtained in the inertial subrange of the hyperviscous solution (slope $= -1.48 \pm 0.05$); the dotted line is the RG prediction (slope $= -1.667$).

power-law region. Therefore, there is a large intermediate subrange, characterized by a constant rescaled energy flux $\Pi(k)/\ln(k)$, which depends on the dissipation mechanism. On the other hand, the spectrum of the viscous simulation shows also a bump of less amplitude which spans over all the range of wave-number. This bump prevents the apparition of any power-law region. These observations may be compared with the results of Leveque and She [15]. They have shown, for a dynamic model of turbulence, that the energy spectrum depends on the hyperviscosity exponent h. Their interpretation of the phenomenon is the following. Even if the energy flux (rescaled in our context) is constant, the dynamics is not just a unidirectional energy cascade. As the energy flow reaches the dissipation cutoff, some part is transmitted into the dissipation subrange and another part is reflected back to the larger scales. Because of the reflected flux, the system is forced to develop large amplitude fluctuations to enforce the correct energy flux imposed by the external forcing. However, contrary to what Leveque and She observed in the dynamic model, the hyperviscous spectrum in Fig. 13(a) shows an inflection point and allows a small power-law subrange to take place. Therefore, if the interpretation of Leveque and She applies in our case, it seems to be "localized" in an intermediate subrange. Another explanation for the energy bump has been given by Eyink [16, 41] who conjectured that it is related to a breakdown of locality in the energy transfer.

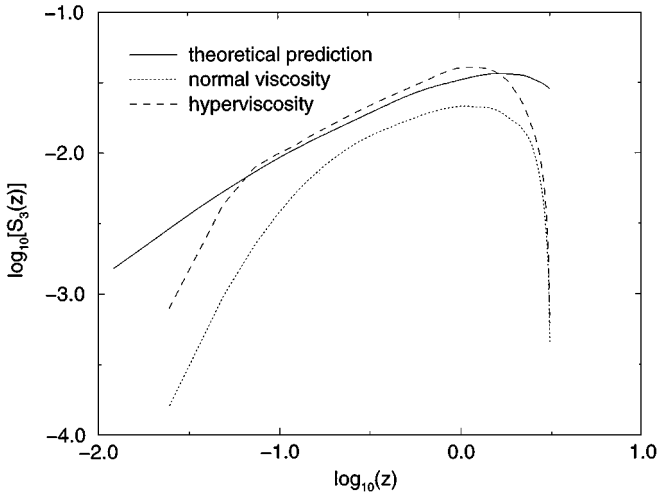

FIG. 14. Third-order structure function $S_3(z)$ for the viscous (dotted lines) and hyperviscous (dashed lines) Navier–Stokes simulations compared to the theoretical prediction (solid line).

We shall now investigate the properties of the flow in physical space. We define the longitudinal velocity increments

$$\delta v_L(z) = v_1(x_1 + z, x_2, x_3) - v_1(x_1, x_2, x_3).$$

Then the structure functions $S_n(z)$ are given by

$$S_n(z) = (-1)^n \langle (\delta v_L(z))^n \rangle,$$

for any integer n. An exact relation for $S_3(z)$ can be derived in the limit of infinite domain size $L \to \infty$ and zero (hyper)viscosity $\nu_h \to 0$,

$$S_3(z) = \frac{6}{z^4} \int_0^z F_{LL}(r) r^4 \, dr, \tag{26}$$

where $F_{LL}(r)$ is the two-point correlation function of the forcing given by Eq. (12). (For the derivation of this equation, see Loitsyanskii's integral in Monin and Yaglom [34].) Note that, if $k_o \to 0$, Eq. (26) becomes $S_3(z) = \frac{4}{5}\varepsilon z$. Figure 14(a) compares the third structure functions $S_3(z)$ computed from the viscous and hyperviscous simulation data with Eq. (26). The discrepancy observed on the left side of the graph is due to the nonvanishing (hyper)viscosity which causes an underprediction of $S_3(z)$, while the discrepancy in the region on the right side is due to the finiteness of the domain. For symmetry reasons, $S_3(z)$, like all odd structure functions, crosses the abscissa axis for $z = \pi$ if the domain is $0 < x < 2\pi$. The agreement is quite good for the hyperviscous simulation. The region of good agreement defines the inertial range in physical space. We see that for the viscous problem, we do not really have an inertial subrange in space. (Recall that we did not have a power-law region in the energy spectrum for that case.)

The question of the nonuniversality of the inertial range scales with respect to the dissipation mechanism can be addressed, in principle, looking at the probability density functions (pdf's) of the longitudinal velocity increment $\delta v_L(z)$ and the lateral (or transverse) velocity increment

$$\delta v_N(z) = v_2(x_1 + z, x_2, x_3) - v_2(x_1, x_2, x_3),$$

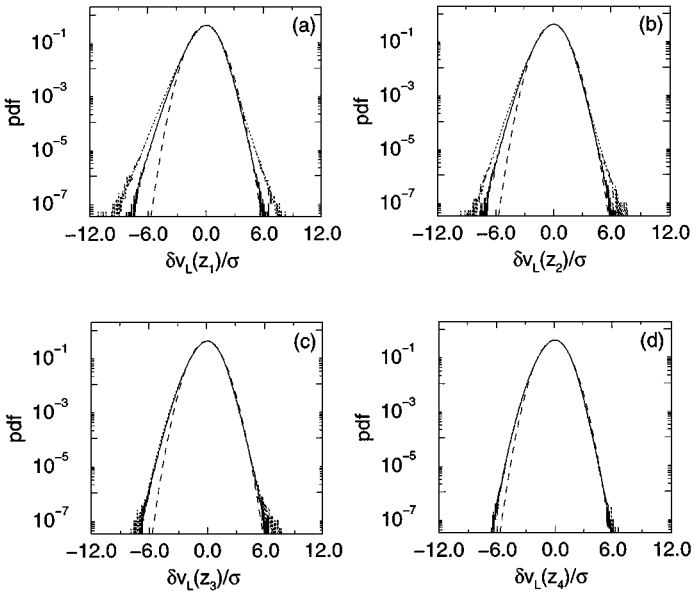

FIG. 15. Normalized probability density functions of the longitudinal velocity increments $\delta v_L(z)$: for $z_i = 4.91 \times 10^{-2}, 9.82 \times 10^{-2}, 1.96 \times 10^{-1}, 3.93 \times 10^{-1}$: Gaussian distribution (dashed lines); viscous simulation (dotted lines); hyperviscous simulation (solid lines).

for simulations with different dissipation terms. To evaluate the probability density functions (Figs. 15 and 16), we have used space distributions, for which we have $\approx 1.68 \times 10^7$ grid point values at each time. Using 40 different realizations, we reach a total of $\approx 6.71 \times 10^8$ values. The dotted lines (resp. solid lines) are the normalized distributions obtained for

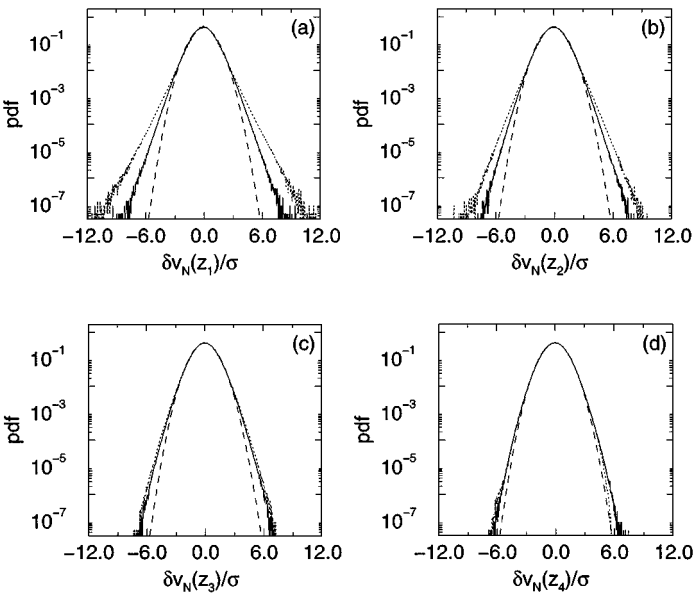

FIG. 16. Normalized probability density functions of the transverse velocity increments $\delta v_N(z)$ for $z_i = 4.91 \times 10^{-2}, 9.82 \times 10^{-2}, 1.96 \times 10^{-1}, 3.93 \times 10^{-1}$: Gaussian distribution (dashed lines); viscous simulation (dotted lines); hyperviscous simulation (solid lines).

the viscous (resp. hyperviscous) simulation (σ is the standard deviation). The increments z_i are chosen in the dissipative subrange and in the inertial subrange. For $z = z_1$ in the hyperviscous case and $z = z_2, z_3, z_4$ in both cases, these distributions display exponential wings. For $z = z_1$ in the viscous case, the tails of the pdf's decrease more slowly than exponentially. For longitudinal increments, the negative wing is stronger than the positive wing. For lateral increments, the distributions are symmetric. For $z = z_4$, a typical inertial range scale, the pdf's for the viscous (dotted lines) and hyperviscous (solid lines) simulations are superimposed. Therefore, no obvious nonuniversality of the inertial range can be detected observing the pdf's.

If we compare our Figs. 15 and 16 with Figs. 7 and 8 of Vincent and Meneguzzi [12], we observe a far less pronounced deviation from the Gaussian shape, which confirms the low values obtained for the velocity derivative skewness and the flatness. In comparison with large-scale forced turbulence, our system has a somewhat different behavior in the dissipative subrange since, for very high wave-numbers, the local Reynolds number is very low and our system combines a linear randomly forced Stokes problem and a weak nonlinear interaction which is responsible for the deviation from the Gaussian distribution. Therefore, we expect to have less strong intermittency than in large-scale forced turbulence. The pdf's of the viscous simulation (dotted lines) versus the hyperviscous one (solid lines) show interesting differences in the dissipative subrange. In the hyperviscous case, the energy flux drops very abruptly in the dissipation subrange. Therefore, we have a weaker nonlinear effect. If we follow the explanation of dissipative scales intermittency given by Frisch and Morf [42], this suggests that since the hyperviscosity leads to a strong damping, the singularities in the complex plane associated to the intermittent burst occur very far from the real axis, and occurrences very close to the real axis have extremely small probabilities.

The last result of this section is the Eulerian frequency spectrum $E_\omega(\omega)$ defined as the Fourier transform of the autocorrelation

$$B(\tau) = \langle v_1(\boldsymbol{x}, t + \tau) v_1(\boldsymbol{x}, t) \rangle.$$

The autocorrelation function has been computed with a set of 60 realizations with a time interval $\Delta t = 0.04$ between each of them. The average is performed over the space domain. We have considered only the hyperviscous simulation. The frequency spectrum is presented in Fig. 17. The slope of the linear least-squares fit is -1.38 ± 0.06 and therefore supports that the random sweeping hypothesis [20] is valid since we have approximately $E_\omega(\omega) \propto E(\omega/v_{rms})$ (see $E(k)$ on Fig. 13).

6. CONCLUSIONS

We have presented two randomly forced turbulence problems, based, respectively, on the one-dimensional Burgers equation and on the three-dimensional incompressible Navier–Stokes equations. For both of these problems, the random forcing is chosen accordingly to the RG theory [5, 7, 33] in order to show a Kolmogorov $-5/3$ energy spectrum in the inertial subrange. The main concern of our work was to design a suitable numerical algorithm to deal with randomly forced turbulent flows and to show some new results obtained using this method. The spatial discretization is achieved by the standard Fourier spectral method. The time integration scheme is a second-order Runge–Kutta method. The choice of this particular scheme presents several advantages: it is more stable than the

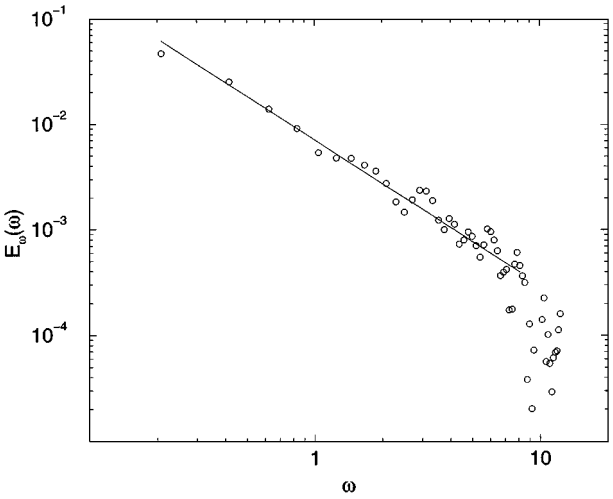

FIG. 17. Eulerian frequency spectrum $E_\omega(\omega)$ (circles) and linear least-squares fit in the inertial range (solid line). The slope of the least-squares fit is -1.38 ± 0.06.

second-order Adams–Bashforth scheme; dealiasing can be performed at no extra computational cost by random shifting; the scheme is readily extended to take into account an additive noise term. A particular attention was devoted to the demonstration of the consistency of the stochastic scheme. Regarding the implementation, we found that the random number generator is a critical issue. We recommend a random number algorithm based on a lagged Fibonacci series. For the Navier–Stokes problem, we have also considered replacing the usual Laplacian dissipation mechanism by a high-order hyperviscous dissipation.

In agreement with the work of Chekhlov and Yakhot [22, 23], an energy spectrum $\propto k^{-5/3}$ is observed for the stochastic Burgers problem in the inertial subrange. In that subrange of wave-numbers, the energy flux is $\propto \ln(k)$. We have also investigated the spatial structure functions $S_n(z)$. For $n = 3$, there is an exact expression valid in the inertial range. The numerical result shows very good agreement with this exact expression. The solution in physical space exhibits very large shocks that evolve slowly. Nonetheless, analyzing the time structure functions, we found that random sweeping is the statistically dominant effect of the large-scale motion on the small-scales. Our simulation has been performed with the usual viscous dissipation and our results, for various statistics, are in very good agreement with those presented by Chekhlov and Yakhot [23] for an hyperviscous system. Contrary to the dynamical model of Leveque and She [15], the statistical properties, in the inertial subrange, do not show any dependence on the dissipation mechanism.

Two Navier–Stokes simulations have been performed. The first one with a normal viscosity and the second one with an hyperviscosity ($h = 8$). The hyperviscous solution shows a bump in the energy spectrum, but the effect appears for a limited range of scales and a power-law inertial subrange spectrum is present. However, this spectrum does not agree with the $k^{-5/3}$ RG prediction. The third-order structure function $S_3(z)$ is in good agreement with the theoretical prediction for the hyperviscous simulation. We have not been able to detect any dependence on the dissipation mechanism in the inertial subrange by comparing the pdf's of the longitudinal and transverse velocity increments for the two simulations. Our calculation of the energy frequency spectrum shows a scaling law which agrees with the random Taylor hypothesis.

Overall, we bring to the attention of the reader that the random force method [1], applied to turbulence, allows us to study idealized models of isotropic turbulence with nonconstant energy flux. This family of problems, which, contrary to constant energy flux turbulence, has not been studied extensively, should receive more interest since the nature of the energy transfer from the mean flow to the turbulence remains an open question and it is possible that, in the presence of strong shear, some energy is injected directly from the mean flow to the small-scale motions of turbulence. The problems studied in this paper are isotropic models for such a turbulence.

Another point which is worth investigating by comparing low wave-number forced turbulence with inertial subrange forced turbulence is how randomness is generated in the small scales. If we compare the solution in physical space obtained with a low wave-number forced Burgers problem [33] with the inertial subrange forced equation presented in this paper, we observe that the degree of randomness achieved by the small scales is only due to the random forcing since the solution of the large-scale forcing case remains very smooth except for the very few points where strong shocks are present. On the contrary, for the Navier–Stokes problem, there are intrinsic instability mechanisms which contribute to the production of randomness [43] and the random forcing comes only as a correction to the energy flux.

APPENDIX

In this Appendix, we illustrate the Ito–Taylor expansion and we give the statement of the proposition related to the convergence properties of the truncated Ito–Taylor series used in Section 3. We shall assume that all the necessary derivatives and multiple integrals exist. The simplest nontrivial Ito–Taylor expansion is obtained if we expand the function $\boldsymbol{a}(s, \boldsymbol{y}(s))$ in Eq. (14) using the Ito formula, Eq. (15). We derive

$$y_l(t+\Delta t) = y_l(t) + \int_t^{t+\Delta t} B_{lj}(s)\, dw_j(s) + a_l(t, \boldsymbol{y}(t))\Delta t + \partial_t a_l(t, \boldsymbol{y}(t))\frac{\Delta t^2}{2} + R_l,$$

with the remainder

$$\begin{aligned} R_l = &\int_t^{t+\Delta t}\int_t^s \partial_i a_l(\tau, \boldsymbol{y}(\tau)) B_{ij}(\tau)\, dw_j(\tau)\, ds \\ &+ \int_t^{t+\Delta t}\int_t^s \partial_i a_l(\tau, \boldsymbol{y}(\tau)) a_i(\tau, \boldsymbol{y}(\tau))\, d\tau\, ds \\ &+ \frac{1}{2}\int_t^{t+\Delta t}\int_t^s \partial_i \partial_k a_l(\tau, \boldsymbol{y}(\tau)) B_{ij}(\tau) B_{kj}(\tau)\, d\tau\, ds \\ &+ \int_t^{t+\Delta t}\int_t^s \partial_t a_l(\tau, \boldsymbol{y}(\tau))\, d\tau\, ds. \end{aligned}$$

Again, we can expand the remainder repeating the procedure of introducing the expansion of $\boldsymbol{a}(s, \boldsymbol{y}(s))$ obtained by the Ito formula. If we iterate this procedure ad infinitum we can write the expansion of $\boldsymbol{y}(t+\Delta t)$ in the general form given by Eq. (16).

We take the truncated Ito–Taylor expansion

$$\boldsymbol{y}^k(t+\Delta t) = \sum_{\boldsymbol{\alpha}\in\mathcal{L}_k} I_{\boldsymbol{\alpha}}[\mathcal{C}_{\boldsymbol{\alpha}}(t,\boldsymbol{y}(t))]_{t,t+\Delta t}.$$

Let us define $C_P^l(\boldsymbol{R}^M, \boldsymbol{R})$, the space of l times continuously differentiable functions $g:\boldsymbol{R}^M \to \boldsymbol{R}$ for which g and all of its partial derivatives of order up to and including l have polynomial growth.

PROPOSITION 1. *We define*

$$\mathcal{L}_k = \{\boldsymbol{\alpha} \mid \Lambda(\boldsymbol{\alpha}) \le k\}.$$

Suppose that $\boldsymbol{a}(\cdot,\cdot)$ *and* $B(\cdot)$ *satisfy some regularity and technical properties. Then, for each* $g \in C_P^{2(k+1)}(\boldsymbol{R}^M, \boldsymbol{R})$, *there exist constants* $K > 0$ *and* $r \in \{1, 2, \ldots\}$ *such that*

$$|\langle g(\boldsymbol{y}^k(t+\Delta t)) - g(\boldsymbol{y}(t+\Delta t))\rangle| \le K(1+|\boldsymbol{y}(t)|^{2r})\Delta t^{k+1}.$$

The complete set of hypotheses and the demonstration of this proposition is given in Kloeden and Platen [32, Proposition 5.11.1].

ACKNOWLEDGMENTS

One of the authors (L.M.) is grateful to A. Chekhlov and S. Gavrilakis for useful conversations, M. Meneguzzi for providing his spectral code, and W. P. Petersen for having read a preliminary version of this manuscript and for providing the random number generator subroutines. The simulations were performed on the computers of the Swiss Center for Scientific Computing, Manno. The work of L. Machiels is supported by the Swiss National Foundation for Scientific Research.

REFERENCES

1. E. A. Novikov, Functionals and the random-force method in turbulence theory, *Soviet Phys. JETP* **20**(5), 1290 (1965).
2. W. D. McComb, *The Physics of Fluid Turbulence* (Clarendon, Oxford, 1990).
3. H. A. Rose, Eddy diffusivity, eddy noise and subgrid-scale modelling, *J. Fluid Mech.* **81**, 719 (1977).
4. D. Forster, D. R. Nelson, and M. J. Stephen, Large-distance and long-time properties of a randomly stirred fluid, *Phys. Rev. A* **16**(2), 732 (1977).
5. C. DeDominicis and P. C. Martin, Energy spectra of certain randomly-stirred fluids, *Phys. Rev. A* **19**(1), 419 (1979).
6. J.-D. Fournier and U. Frisch, Remarks on the renormalization group in statistical fluid dynamics, *Phys. Rev. A* **28**(2), 1000 (1983).
7. V. Yakhot and S. A. Orszag, Renormalization group analysis of turbulence. I. Basic theory, *J. Sci. Comput.* **1**(1), 3 (1986).
8. W. D. McComb and A. G. Watt, Conditional averaging procedure for the elimination of the small-scale modes from incompressible fluid turbulence at high Reynolds numbers, *Phys. Rev. Lett.* **65**(26), 3281 (1990).
9. S. A. Orszag and G. S. Patterson, Numerical simulation of three-dimensional homogeneous isotropic turbulence, *Phys. Rev. Lett.* **28**(2), 76 (1972).
10. E. D. Siggia, Numerical study of small-scale intermittency in three-dimensional turbulence, *J. Fluid Mech.* **107**, 375 (1981).
11. R. M. Kerr, Higher-order derivative correlations and the alignment of small-scale structures in isotropic numerical turbulence, *J. Fluid Mech.* **153**, 31 (1985).

12. A. Vincent and M. Meneguzzi, The spatial structure and statistical properties of homogeneous turbulence, *J. Fluid Mech.* **225**, 1 (1991).
13. V. Borue and S. A. Orszag, Forced three-dimensional homogeneous turbulence with hyperviscosity, *Europhys. Lett.* **29**(9), 687 (1995).
14. V. Borue and S. A. Orszag, Self-similar decay of three-dimensional homogeneous turbulence with hyperviscosity, *Phys. Rev. E* **51**(2), R856 (1995).
15. E. Leveque and Z.-S. She, Viscous effects on inertial range scalings in a dynamical model of turbulence, *Phys. Rev. Lett.* **75**(14), 2690 (1995).
16. G. L. Eyink, The renormalization group method in statistical hydrodynamics, *Phys. Fluids* **6**(9), 3063 (1994).
17. L. M. Smith and W. C. Reynolds, On the Yakhot–Orszag renormalization group method for deriving turbulence statistics and models, *Phys. Fluids A* **4**(2), 364 (1992).
18. V. Yakhot, S. A. Orszag, and Z.-S. She, Space-time correlations in turbulence: Kinematical versus dynamical effects, *Phys. Fluids A* **1**(2), 184 (1989).
19. H. Tennekes, Eulerian and Lagrangian time microscales in isotropic turbulence, *J. Fluid Mech.* **67**, 561 (1975).
20. S. Chen and R. H. Kraichnan, Sweeping decorrelation in isotropic turbulence, *Phys. Fluids A* **1**(12), 2019 (1989).
21. M. Nelkin and M. Tabor, Time correlations and random sweeping in isotropic turbulence, *Phys. Fluids A* **2**(1), 81 (1990).
22. A. Chekhlov and V. Yakhot, Kolmogorov turbulence in a random-force-driven Burgers equation, *Phys. Rev. E* **51**(4), R2739 (1995).
23. A. Chekhlov and V. Yakhot, Kolmogorov turbulence in a random-force-driven Burgers equation: Anomalous scaling and probability density functions, *Phys. Rev. E* **52**(5), 5681 (1995).
24. A. A. Migdal, S. A. Orszag, and V. Yakhot, Intrinsic stirring force in turbulence and the ϵ-expansion, unpublished, Princeton University.
25. R. Panda, V. Sonnad, E. Clementi, S. A. Orszag, and V. Yakhot, Turbulence in a randomly stirred fluid, *Phys. Fluids A* **1**(6), 1045 (1989).
26. C. E. Leith, Stochastic backscatter in a subgrid-scale model: Plane shear mixing layer, *Phys. Fluids A* **2**(3), 297 (1990).
27. D. Carati, S. Ghosal, and P. Moin, On the representation of backscatter in dynamic localization models, *Phys. Fluids* **7**(3), 606 (1995).
28. C. Canuto, M. Y. Hussaini, A. Quarteroni, and T. A. Zang, *Spectral Methods in Fluid Dynamics* (Springer-Verlag, New York, 1988).
29. S. L. Anderson, Random number generators on vector supercomputers and other advanced architectures, *SIAM Rev.* **32**(2), 221 (1990).
30. W. P. Petersen, Lagged Fibonacci series random number generators for the NEC SX-3, *Int. J. High Speed Comput.* **6**(3), 387 (1994).
31. W. P. Petersen, *Some Evaluations of Random Number Generators in Real*8 Format*, Technical Report TR-96-06, Swiss Center for Scientific Computing, April 1996.
32. P. E. Kloeden and E. Platen, *Numerical Solution of Stochastic Differential Equations* (Springer-Verlag, Berlin, 1992).
33. A. Chekhlov, *Studies of Forced-Dissipative Turbulence in Model Hydrodynamics*, Ph.D. thesis, Princeton University, May 1995.
34. A. S. Monin and A. M. Yaglom, *Statistical Fluid Mechanics: Mechanics of Turbulence* (MIT Press, Cambridge, MA, 1975), Vol. 2.
35. W. P. Petersen, Some experiments on numerical simulations of stochastic differential equations and a new algorithm, *J. Comput. Phys.* **113**, 75 (1994).
36. R. S. Rogallo, *An ILLIAC Program for the Numerical Simulation of Homogeneous, Incompressible Turbulence*, Technical Report TM-73203, NASA, 1977.
37. D. E. Knuth, *The Art of Computer Programming. Vol. 2. Seminumerical Algorithms* (Addison–Wesley, Reading, MA, 1981).

38. I. Vattulainen, T. Ala-Nissila, and K. Kankaala, Physical tests for random numbers in simulations, *Phys. Rev. Lett.* **73**(19), 2513 (1994).
39. A. Papoulis, *Probability, Random Variables and Stochastic Processes* (McGraw–Hill, New York, 1991).
40. G. K. Batchelor, *The Theory of Homogeneous Turbulence* (Cambridge Univ. Press, Cambridge, 1953).
41. G. L. Eyink, Energy dissipation without viscosity in ideal hydrodynamics. I. Fourier analysis and local energy tranfer, *Phys. D* **78**, 222 (1994).
42. U. Frisch and R. Morf, Intermittency in nonlinear dynamics and singularities at complex times, *Phys. Rev. A* **23**(5), 2673 (1981).
43. L. Machiels, Predictability of small-scale motion in isotropic fluid turbulence, *Phys. Rev. Lett.* **79**(18), 3411 (1997).